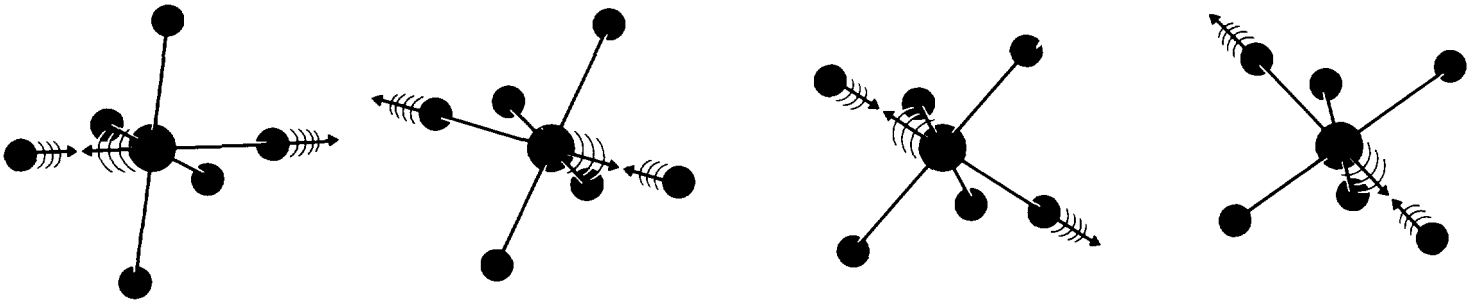

the modern revolution in

by Robin S. McDowell, Chris W. Patterson, and William G. Harter

Lasers have revealed a surprising order to the complex motions of vibrating, rotating molecules.

One of the most exciting challenges in modern science has been to unravel the detailed code of molecular spectra because this code speaks directly of a molecule's energy levels. In other words, the allowed energies and motions of a molecule can be delicately probed by seeing which photons of known frequency tickle the molecule into excited states. In particular, to understand the vibrational motions important for chemical reactions, it is necessary to decipher the portion of the electromagnetic spectrum called the infrared (see sidebar "The Absorption Spectrum-The Signature of Molecular Motions").

However, the infrared spectra of highly symmetric molecules, even of those with only a half dozen or so atoms, appear at first to be a hopeless jumble of finely spaced energy transitions. In fact, only ten years ago the sight of the thousands upon thousands of tine absorption peaks massed together in each absorption band of octahedrally or tetrahedrally symmetric molecules, such as UF_6 or SiF_4, was enough to make an experienced spectroscopist blanch. But spectroscopists persevered and, using lasers as a source of precisely tuned infrared photons, discovered patterns with surprising order. This newly found order not only makes possible the detailed assignment of each absorption peak to a specific energy transition, but also increases our understanding of the allowed motions of these molecules. As it turns out, it is the high degree of molecular symmetry that accounts for both the array of closely spaced transitions and the ordered pattern of absorption.

The spur to this breakthrough has been laser photochemistry. In particular, knowledge gained about the vibrations of the octahedral molecule uranium hexafluoride (UF_6) has been useful in designing the Los Alamos molecular isotope separation process for uranium. Since the initial, isotonically selective step in this process is vibrational excitation of UF_6, an understanding of its infrared spectrum is imperative. This is especially true for the heavy, symmetric UF_6 molecules since the vibrational frequencies of the various isotopic species differ by only small amounts and since there is considerable overlap in the complex array of possible absorption.

Moreover, one version of the separation processes involves driving the molecule into a high state of excitation, to the point of dissociation. An understanding of this process requires knowledge of the full ladder of energy levels, not just of the lower rungs.

To achieve such excitation, each molecule must absorb many photons. This multiple-photon process involves intense radiation fields that drive populations of molecules up and down the vibrational energy ladder. Thus the rates at which molecules change their vibrational motion become important.

Although infrared spectroscopy was an already mature and well-established field of research, its capabilities, both theoretical and experimental, were challenged by the need to understand these phenomena. Fortunately, the recent advances in designing lasers as tunable sources of very-narrow-linewidth infrared radiation revolutionized this field, and theoretical developments accelerated to keep pace. This article discusses the comprehensive unraveling of the infrared spectrum for the first step up the vibrational energy ladder and the determination of the next few rungs; the article "Multiple-Photon

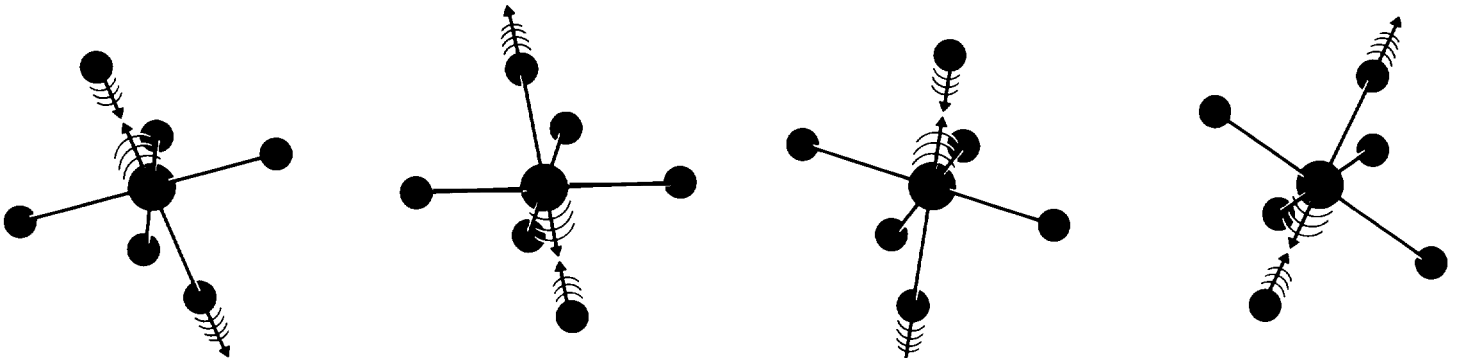

infrared spectroscopy

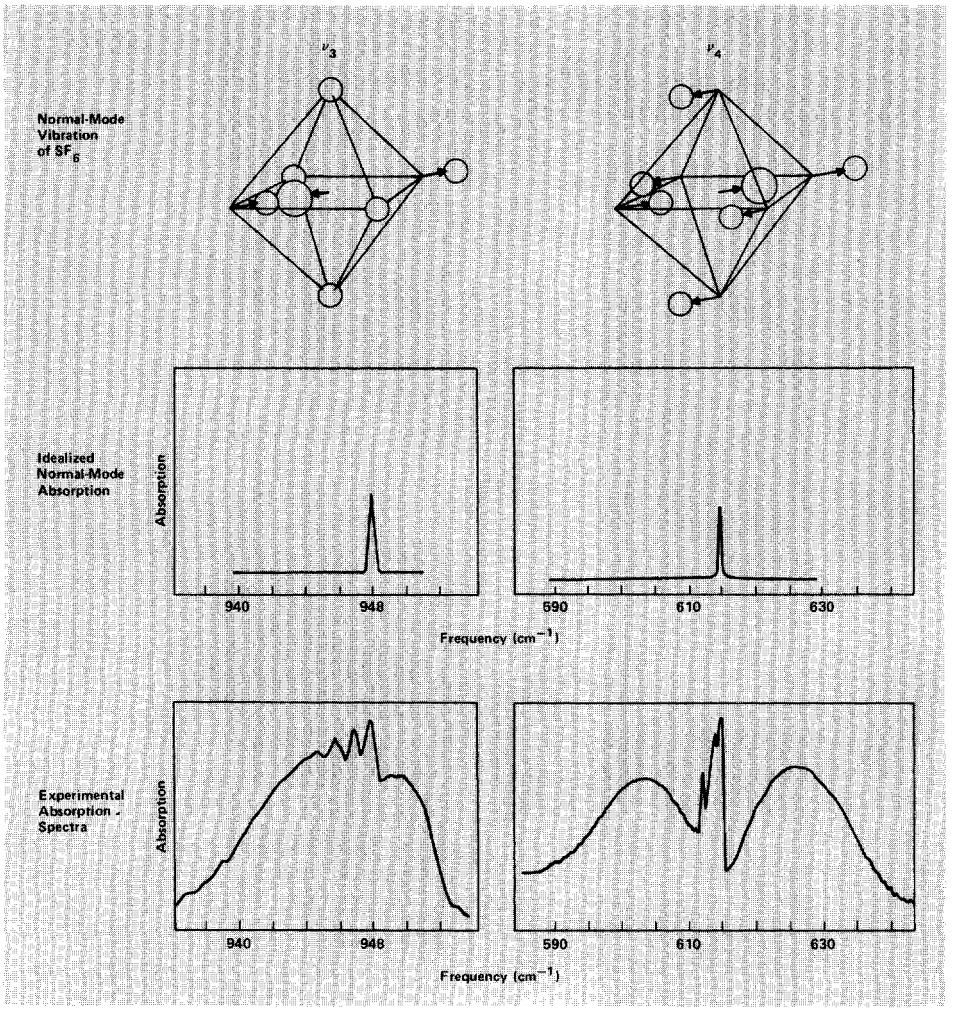

Fig. 1. The two infrared-active vibrations of SF_6 and associated spectra. The ν_3 normal mode is principally an S-F bond stretching motion, whereas the ν_4 mode is an F-S-F bending motion. If these vibrations were harmonic and no molecular rotation occurred, then the spectra would look like the graphs labeled Idealized Normal-Mode Absorption. Much of the width and structure seen in the Experimental Absorption Spectra are due to small rotational energy changes that accompany the large change in vibrational energy. (All spectra in this article have absorption increasing in the up direction.)

Excitation" in this issue deals with excitation to dissociation in the presence of intense radiation fields.

The Complexity of Molecular Motion

People not familiar with modern infrared spectroscopy are apt to picture a vibrating molecule as a collection of atomic point masses held together by rather rigid springs. In fact, much infrared spectroscopy has been based on just such a model. The rigid springs allow only small oscillations about equilibrium, resulting in new-harmonic vibrations. Moreover, the molecule vibrates with only a certain number of characteristic motions, or normal modes, that are independent of each other. The particular frequency of a mode depends on the strengths or force constants of the bonds that are stretching or bending and on the masses of the atoms that are moving. This model is justified by the fact that the normal modes that interact with radiation are easily identified at low resolution as absorption peaks in either infrared spectra or Raman radiation-scattering spectra.

Figure 1 shows the ν_3 and ν_4 vibrational modes for sulfur hexafluoride (SF_6) along with their infrared absorption spectra. As can be seen, the experimental absorption peaks have considerable width and structure compared to the idealized absorption of normal-mode vibrations. This structure is typical and is due primarily to small changes in rotational energy that occur simultaneously with the larger changes in vibrational energy. The basic pattern of rotational energy levels can be explained using as a model the same rigid molecule, but now rotating. In this approach the rotational

continued on page 42

the absorption spectrum-

SIDEBAR 1:

the signature of molecular motions

Photons absorbed by a molecule induce transitions, separately or in combination, between its quantized rotational, vibrational, and electronic energy states. Rotational energy states involve motions of a molecule that produce a net angular momentum about its center of gravity. Vibrational energy states involve oscillations of the nuclei about the center of gravity. And electronic energy states involve motions of the bonding electrons. Therefore, encoded in a molecule's absorption spectrum is much information about its dynamics and structure. The basis for decoding this information is the fact that the energy of an absorbed photon equals the difference between two of the molecule's energy states.

One can approximate the energy difference ΔE between two adjacent rotational energy states of a gaseous molecule by assuming that the molecule is a rigid rotor, that is, by assuming that no molecular deformation accompanies the rotation. Then,

$$\Delta E = \left(\frac{h}{2\pi}\right)^2 \frac{J+1}{I} ,$$

where the rotational quantum number J can assume any nonnegative integral value and I is the molecule's moment of inertia about the axis of rotation. Note that ΔE is inversely proportional to Z and increases with increasing J. Numerical values of ΔE based on reasonable estimates of I correspond to the energies of photons in the microwave and far infrared. Thus, the absorption spectrum of a molecule in this region provides information about its moment of inertia, that is, about bond lengths and bond angles.

Vibrational energy states are regarded as being the result of bending or stretching of individual bonds, skeletal motions of the molecule as a whole, or combinations and overtones of these motions, For a diatomic molecule the energy difference between two adjacent vibrational states in the harmonic oscillator approximation is given by

$$\Delta E = \frac{h}{2\pi} \left(\frac{k}{\mu}\right)^{1/2} .$$

Here μ is the reduced mass of the vibrating nuclei, and k is the proportionality constant between the restoring force and the displacement. (Note that the assumption of harmonic oscillation leads to a constant energy difference between vibrational levels, a prediction that is not borne out by experiment.) For reasonable estimates of k, numerical values of ΔE correspond to those of photons in the mid and near infrared. This portion of a molecule's absorption spectrum thus provides information about restoring forces, that is, about bond strengths.

Since photons in the mid and near infrared have sufficient energy to induce rotational transitions along with vibrational transitions, rotational tine structure is associated with each vibrational absorption feature of a gaseous molecule. Therefore, the rotational-vibrational absorption spectrum also yields much of the information available from the pure rotational spectrum and is of particular interest to molecular spectroscopists. In addition, this spectrum is a powerful tooI for qualitative and quantitative analysis.

Photons in the ultraviolet with still higher energies induce transitions between electronic energy states. Thus, the ultraviolet absorption spectrum reveals information about the forces binding valence electrons in molecules, Both vibrational and rotational fine structures are superimposed on the electronic transitions, but this spectrum is more difficult to decode than the rotational-vibrational spectrum,

Shown here are the infrared and adjacent portions of the electromagnetic spectrum. The term infrared radiation refers to radiation with wavelengths between the red limit of the visible spectrum at 0.8 micrometer (μm) and the beginning of the microwave region at 1000 Wm. The infrared spectrum thus covers a factor of 1250 in wavelength; in contrast, the extreme limits of sensitivity of the human eye cover only a factor of 2.

Infrared radiation is usually characterized by its wavenumber, or reciprocal wavelength, rather than by its frequency or wavelength. Further, it is customary to use the reciprocal centimeter (cm-l) as the wavenumber unit. Somewhat confusingly, both wavenumber and frequency are designated by the symbol v. The two quantities are, of course, related by the speed of light, $\nu(\mathrm{cm}^{-1}) = \nu\,(\mathrm{hertz})/c$, so that $1\ \mathrm{cm}^{-1} \simeq 30{,}000$ megahertz. ■

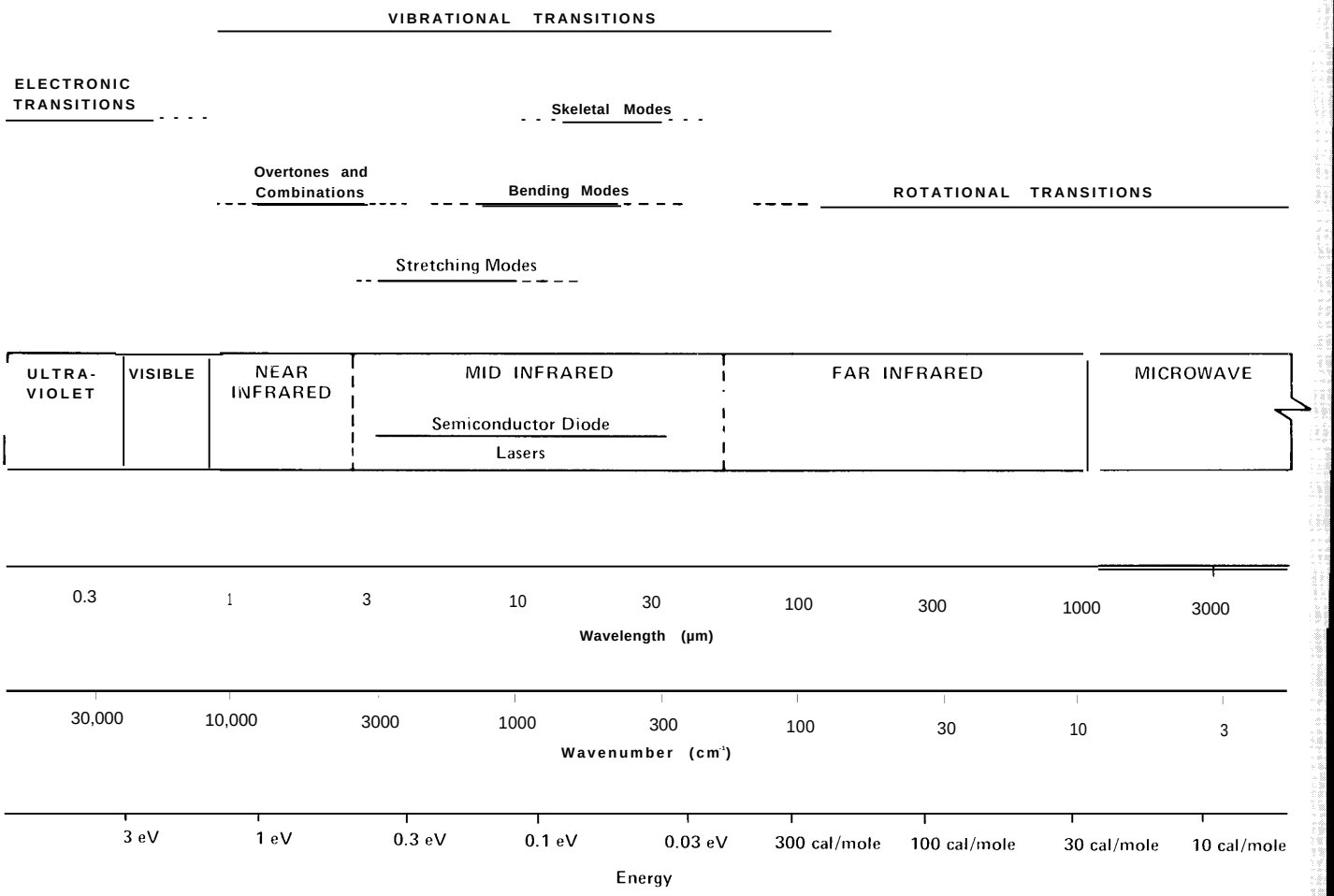

Depending on the energy of a photon, its absorption by a molecule can give rise to rotational, vibrational, or electronic transitions. The energy of a photon equals the product of its frequency and Planck's constant or, equivalently, the product of its wavenumber, Planck's constant, and the speed of light. Various units are used for photon energies. Listed here are electron volts (eV), the customary unit in the ultraviolet, visible, and mid- and near-infrared regions, and calories per mole of photons (cal/mole), the customary unit in the far-infrared and microwave regions.

continued from page 39

energy levels are determined independently of the vibrational motion and then simply superimposd on each vibrational level.

Although this model goes a long way toward describing the energy levels of simple molecules, spectroscopists have always realized there are several approximations inherent in the approach. Especially important is the fact that the various motions of a molecule are not fully independent. For example, when a molecule is both rotating and vibrating, the linear vibrational motion of an atom is subject to the pseudo-forces (centrifugal and Coriolis) of a rotating coordinate system. These forces alter the purely rotational or purely vibrational motion of the molecule.

Also, different molecular motions are coupled through anharmonicities. When the bonding force constraining the motion of an atom is not strictly linear with displacement, the vibration will not be strictly harmonic. The anharmonicities are accounted for with nonlinear terms. When applied as corrections to the simple model, these terms account for the presence in the spectra of overtone and combination frequencies of the normal modes. The enharmonic terms also result in shifts of energy levels and in splitting of states that have approximately the same energy.

The end result of these various effects is that an absorption cannot be represented simply as a vibrational transition with a set of rotational transitions superimposed. Rather, the closer one looks at the spectrum, the more complex it appears, and the more the approximations have to be dealt with in order to understand the detail.

Spectroscopic Resolution

Critical to understanding the detail is the concept of resolution. How close can two spectral features be in frequency and still be distinguished? The more detail we can measure in the spectrum, the more we can hope to understand.

Until recently infrared spectra could only be obtained by methods that, though more sophisticated, are not basically different from those employed in the nineteenth century: the infrared radiation from a glowing source (similar to the heating element on an electric stove) is passed through the sample and then dispersed into its various constituent wavelengths by a prism or diffraction grating. This provides resolutions from about 1 cm-l for commercial grating spectrometers down to 0.1 cm^{-1} or slightly less for some specially built instruments. More recently, interferometry has done somewhat better; in this technique there is no dispersion, but instead the interference between two light beams results in an interferogram from which the desired spectrum can be recovered by performing a Fourier transform. The resolution of Fourier-transform infrared spectrometers varies from about 0.05 cm–l for commercially available interferometers to better than 0.01 cm-l in a very few research instruments.

We see, then, that these conventional spectroscopic techniques can divide the infrared region into at most a few hundred thousand resolved elements. This is a considerable number (the human eye can discriminate only about 200 different visible wavelengths), but much spectral detail of all but the simplest molecules will still be concealed, for the widths of the absorption peaks are much less than these resolutions. Several phenomena contribute to the linewidths, but in a low-pressure gas the dominant broadening mechanism is the Doppler effect caused by the thermal motion of the molecules. The magnitude of the Doppler broadening depends upon the molecular mass, the temperature, and the transition frequency, and is typically between 0.01 and 10^{-4} cm-l. Thus an absorption feature that even the best interferometers show as simply a single "line" may actually consist of many individual transitions that could be revealed with increased resolution.

Over the last decade several different infrared laser sources have been developed (see sidebar "Tunable Lasers—The Tools of the Trade") that combine very narrow linewidths with tunability, so that spectra can be obtained by simply passing the laser emission through the sample and recording the intensity of the transmitted light as the wavelength of the source is changed. Because these devices may have linewidths of the order of $1O^{-5}$ to 10^{-6} cm-l, they can effectively divide the infrared region into several *billion* slices. Furthermore, some of these lasers have enough power to saturate the molecular transition being pumped; as will be discussed in more detail below, this phenomenon can be exploited to obtain spectra whose resolution is not limited even by Doppler broadening.

Figure 2 shows the rich detail revealed in the ν_3 absorption spectra of SF_6 as resolution is increased. Spectrum (a) demonstrates the limited resolution of most grating spectrometers; only a few distinct features are visible. The Fourier-transform infrared trace in spectrum (b) has a resolution of 0.06 cm^{-1} but still does not reveal the underlying structure. The third spectrum is a portion of the ν_3 band at Doppler-limited resolution obtained with a tunable diode laser. Now the true complexity of the band becomes apparent. Some of the rotational-vibrational structure is further resolved in the saturation spectrum (d), in which the Doppler limit is surpassed and a resolving power (the ratio of frequency to resolution, $\nu/\Delta\nu$) of 10^9 is achieved. A plot of the whole ν_3 band at the scale of spectrum (d) would require over a mile of paper; some 10,000 transitions in this band have been observed and assigned. The capability of obtaining spectra such as those in (c) and (d) presents both new opportunities and new challenges to infrared spectroscopists, and such data are providing us with important new insights into molecular structure and dynamics.

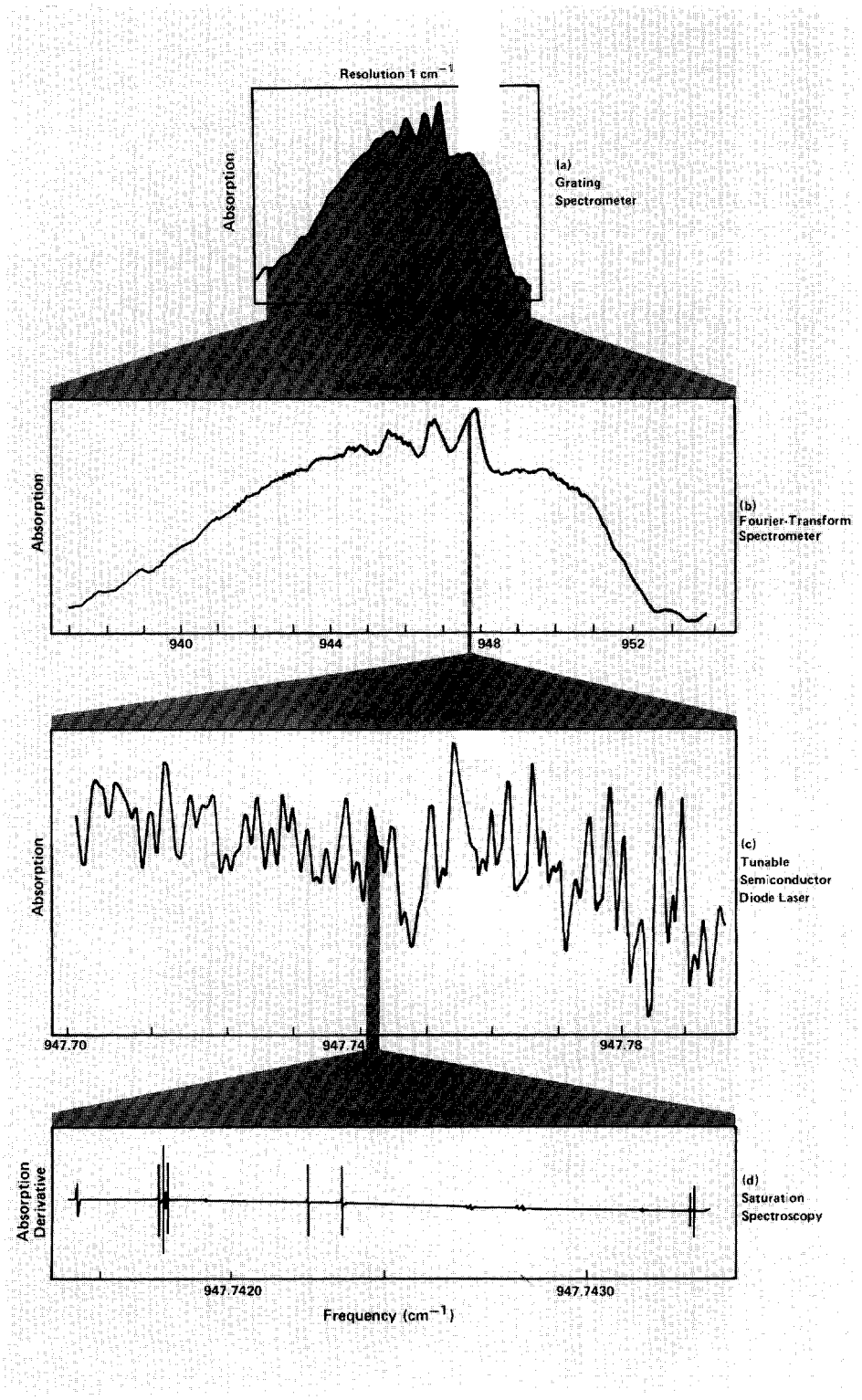

Fig. 2. Infrared spectra of the ν_3 absorption of SF_6 at four resolutions. Spectrum (a) was recorded with a Fourier-transform infrared (FTIR) interferometer, but resolution was degraded to 1 cm-' to match the spectrum produced by a typical commercial grating spectrometer. (b) An FTIR spectrum at a resolution of 0.06 cm-'. (c) A Doppler-limited spectrum obtained by E. D. Hinkley at the MIT Lincoln Laboratory in 1970 using a tunable semiconductor diode laser. The effective resolution is the Doppler linewidth of 0.001 cm-'. (d) Sub-Doppler saturation spectrum recorded by L. Henry at the University of Paris in 1976 with a resolution of better than 10^{-6} c m^{-1}. All of the features in (d) occur inside the small range of frequency possible for the lasting of a single line of a $C0_2$ gas laser. The trace shows the first derivative of the absorption. Each absorption feature shown in (c) and (d) can be assigned to specfic rotational-vibrational transitions of the SF_b molecule.

tunable lasers-the tools of the trade

SIDEBAR 2:

Molecular spectroscopy has undergone its modern revolution to the tune of lasers whose frequencies can be varied continuously over portions of the infrared spectrum. The most widely useful of such lasers are semiconductor diode lasers, which are similar to the light-emitting diodes familiar from so many display applications. These lasers are characterized by highly monochromatic and widely tunable output frequencies. They are also inexpensive and, although requiring cooling to very low temperatures, simple to operate.

The lasing medium of these devices is a D-n junction diode formed in a small crystalline semiconductor. The crystal itself, no bigger than a grain of sand, is mounted on a copper base that serves as an electrical ground and as a thermal connection to a liquefied gas. An injection current applied across the diode causes migration of conduction-band electrons from the n-type material and of holes (valence-band electron vacancies) from the p-type material into the junction region. There the conduction electrons combine with the holes and emit photons whose frequency depends on the energy difference between the valence and conduction bands of the semiconductor.

The diode lases spontaneously on wavenumbers ranging over several tens of reciprocal centimeters. Within this interval particular wavenumbers (cavity modes) can be amplified by constructive interference within an optical cavity. Such an optical cavity is conveniently at hand in the form of the optically flat and parallel cleaved faces of the crystal. The lasing frequency is thus determined by the index of refraction and length of the crystal Because these parameters are temperature dependent, the laser can be tuned by varying the temperature of the crystal. In practice this is accomplished by varying the injection current and hence the electrical energy dissipated within the crystal. A semiconductor diode laser can be continuously tuned in this manner over an interval of about 1 cm^{-1}. Adjacent intervals can be accessed by changing the crystal's thermal or magnetic environment, both of which alter not only the index of refraction and length of the crystal but also the diode's spontaneous emission frequency. With these techniques some semiconductor diode lasers can be quasi-continuously tuned over intervals of 100 cm^{-1} with a linewidth of $1O^{-s}$ $c\,m^{-1}$ or better. However, achieving such a broad tuning range and narrow linewidth requires great care in the fabrication of the diodes, a process involving sophisticated masking and epitaxial growth techniques.

Particularly useful for infrared spectroscopy are semiconductor diode lasers whose spontaneous emission frequency can be varied by altering the chemical composition of the semiconductor from which they are fabricated. For example, lasers made from the semiconductor $Pb_{1-x}Sn_xTe$ (where) $\leq x \leq 0.28$) can be tailored to emit between 6.6 and 33 μm (between 1520 and 300 cm^{-1}).

This brief account of semiconductor diode lasers has overlooked certain of their faults. Generally, the simultaneous lasing of several different cavity modes, separated by about 1 cm-', requires the use of a grating spectrometer to select a single mode. Also, competition between the different cavity modes sometimes causes discontinuous frequency jumps, called mode hops, during a scan. Nevertheless, no other laser is so generally useful for high-resolution spectroscopy throughout a very interesting portion of the infrared region. ■

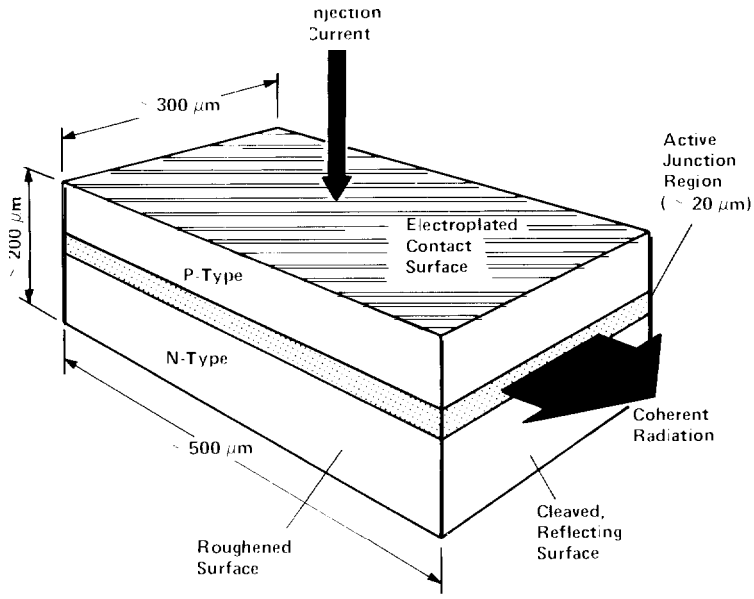

Simplified diagram of a semiconductor diode laser. These tunable lasers have become the workhorses for molecular spectroscopy because of their broad coverage of the infrared region in which rotational-vibra tional transitions occur.

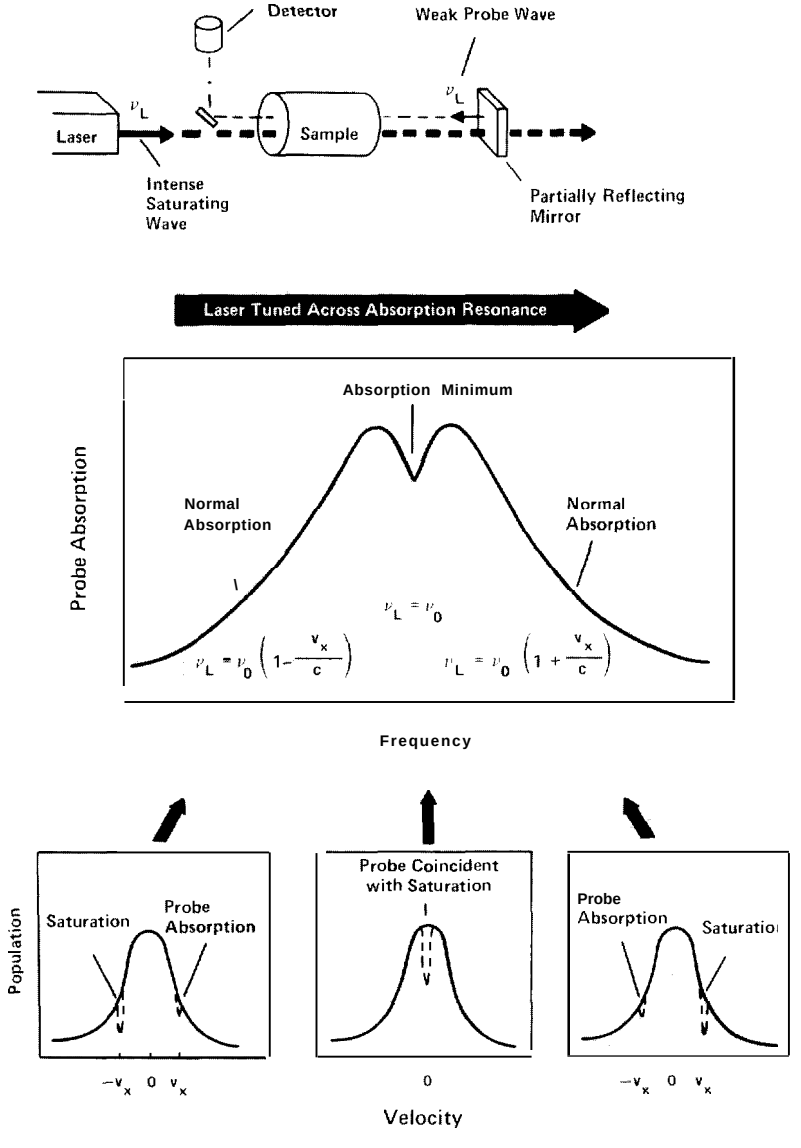

Fig. 3. Saturation spectroscopy. An intense laser at frequency v_L is tuned across a Doppler-broadened absorption. A small part of this saturating wave is reflected back through the sample as a probe wave. If v_L does not match the resonance frequency v_0 of the absorption, the probe and saturating waves see opposite and so different subsets of the velocity distribution and the probe is absorbed normally. If $v_L = v_0$, then the two waves see the same subset of the velocity distribution, the saturating wave has already depleted the population of that subset, and the probe absorption is reduced. The result is a sharp absorption minimum at the resonance frequency.

Sub-Doppler Spectroscopy

Semiconductor diode lasers and other similar devices have narrower bandwidths than the Doppler linewidth and thus represent a significant advance in infrared instrumentation because they allow spectra to be resolved to the Doppler limit. However, is it possible to circumvent this limit and improve resolution still further? Figure 2d demonstrates that it is. The technique of saturation spectroscopy allows one to examine just those molecules in a particular velocity group rather than the whole thermal distribution. The resulting elimination of Doppler broadening can reveal a wealth of additional spectral detail.

Saturation spectroscopy is conceptually very simple. Say a narrow linewidth laser beam tuned to frequency v, is passed in the positive *x* direction through a sample with an absorbing transition centered at frequency v_o. As previously mentioned, the broad thermal distribution of molecular velocities gives the absorption a Doppler linewidth that can be much larger than the laser linewidth. A molecule moving in the *x* direction with velocity v_x, will absorb only photons with a frequency $v_0(1 + v_x/c)$, where the Doppler shift $v_o v_x/c$ exactly compensates for the difference between the laser frequency and the absorption center, $v_L - v_o$. Molecules moving in the opposite direction will absorb only photons with a lower frequency $v_0(1 - v_x/c)$.

If the laser is sufficiently intense, it can excite molecules out of the lower rotational-vibrational state faster than they can return to that state through relaxation mechanisms such as spontaneous emission and collisional energy transfer. The transition is then said to be saturated: the laser has "burned" a hole in the Doppler distribution of the lower state, depleting those molecules whose velocity allows them to absorb the laser radiation.

Suppose now that a partially reflecting mirror at the far end of the sample cell returns part of the laser beam back through

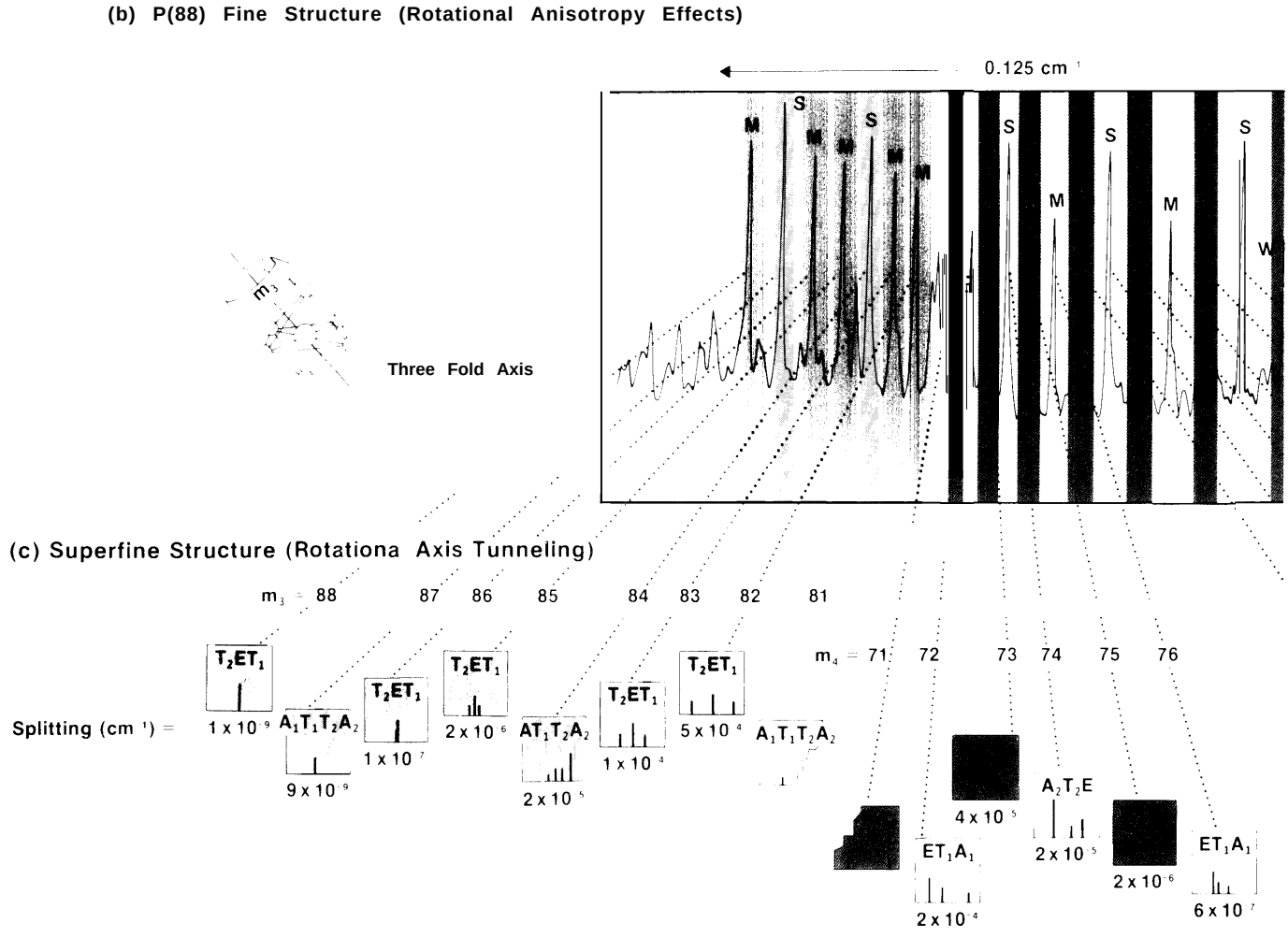

Fig. 4. The bending fundamental v_4 of SF_6 and its splitting patterns. (a) The gross rotational structure as recorded with a Fourier-transform infrared interferometer at a resolution of 0.04 cm^{-1}. The various rotational-vibrational lines in the P *and* R *branches [designated P(J) and* R(J)*] are separated from each other by approximately 0.222 cm^{-1}. The hot- band peaks are v_4 vibrational transitions that start in an excited vibrational state. (b) Doppler-limited spectrum obtained with a tunable diode laser by K. C. Kim and W. B. Person that shows extensive splitting of the P(88) absorption peak. Here the splitting can be attributed to rotational-anisotropy effects; that is, rotation about different axes of the octahedrally symmetric SF_6 molecule results in different amounts of centrifugal distortion. (c) Sketches of superfine structure of the component*

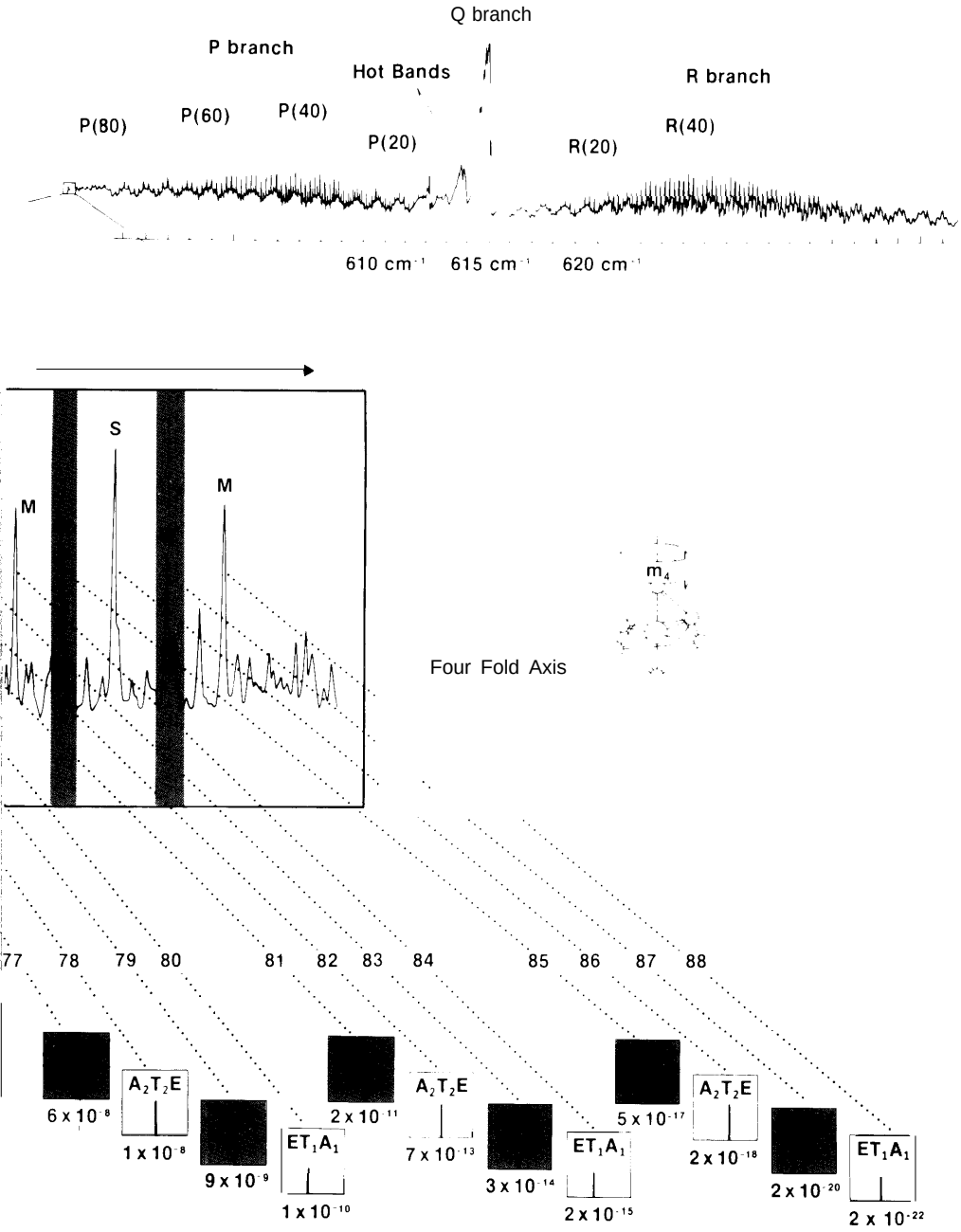

"lines" in P*(88), a result of quantum mechanical tunneling from one equivalent rotational axis orientation to another. Resolution of this structure requires sub-Doppler spectroscopy, which has not yet been done on this band. However, a* T_2ET_1 *triplet similar to what would be observed for* $m_3 = 82, 83, 85, 86,$ and 88 is shown at 947.7417 cm^{-1} *in Fig. 2d; it belongs to* Q*(38) of* ν_3 *with* $m = 38$. *The absorption peaks in (b) that cannot be assigned to a cluster in (c) are hot-band transitions. The color code used in the figure for the clusters (ATE—light yellow, TT—dark blue, TET—light blue, and ATTA—pink) is the result of mixing the three colors that have been assigned to the three kinds of symmetry species (A—red, E—green, and T—dark blue). This code is also used in Figs. 7 and 14.*

the cell as a probe wave (Fig. 3). Since the saturating and probe wave have the same frequency but opposite directions, the returning probe wave will interact with different molecules whose velocity component v_x is opposite to that of the molecules pumped by the saturating beam. This means the probe will be absorbed normally.

If the source is tuned to coincide with the transition frequency v_o, then the probe will sample a population of molecules whose lower states have just been depleted by the saturating wave. Both beams are then interacting with molecules of the same velocity subset, that for which $v_x = O$. As a result, the absorption of the probe wave will be reduced. Thus, as the laser is tuned across the Doppler-broadened line, there will be a sharp resonance absorption minimum at exactly the center frequency v_o. The features shown in Fig. 2d are the derivative traces of such resonances, and the enhanced detail is obvious: over a dozen transitions can be discerned, all of which appear as a single absorption line in the Doppler-limited spectrum of Fig. 2c.

Infrared Spectral Patterns

Infrared spectra range in complexity from a single band of perhaps 20 rotational-vibrational transitions for a light diatomic molecule to the tens of thousands of discrete transitions for heavy polyatomic molecules. The new laser spectroscopy is essential for determining the detailed energy levels of this latter class of molecules. However, even the most complex spectra directly reflect individual physical properties and the allowed motions of the molecule. Our discussion will endeavor to make clear this connection by considering in some detail the spectrum of the octahedrally symmetric molecule SF_6. In addition to having considerable scientific interest in its own right, SF_6 has become the prototype for research on the laser photochemistry and laser isotope separation of such molecules as UF_6.

Since a single atom can move in any of three orthogonal directions, the motion of a molecule composed of N atoms has $3N$ degrees of freedom. Three of these are sufficient to describe the translational motion through space of the center of mass of the molecule, and three more are required to specify its rotational motion (two, if the molecule is linear). There remain $3N - 6$ ($3N - 5$ for linear molecules) vibrational degrees of freedom, which are the fundamental vibrational frequencies or normal modes.

If the molecule is symmetric to the extent of having at least one threefold or higher symmetry axis, then some of these normal modes will occur at the same frequency and are said to be degenerate. Furthermore, for symmetric molecules some of the fundamentals may not induce a change in the molecular dipole moment during the course of a vibration, and thus, according to classical electrodynamics, these fundamentals can not absorb radiation. Such ''infrared-inactive" fundamentals may appear as frequency shifts in the spectrum of scattered light (the Raman effect), or, less commonly, they may be totally inactive except in combination with other modes. These considerations will reduce the number of fundamentals seen in the infrared spectrum, though, if inactive modes and degeneracies are properly counted, the total vibrations will always number $3N - 6$ (or $3N - 5$).

For SF_6, the $3N - 6 = 15$ vibrational degrees of freedom are distributed among one nondegenerate Raman-active mode, one doubly-degenerate Raman-active mode, and four triply-degenerate modes of which two are infrared-active, one is Raman-active, and one is inactive. The two infrared-active fundamentals are called v_3 and v_4, and the low-resolution contours of their absorption bands were shown in Fig. 1.

ROTATIONAL STRUCTURE. In Fig. 4 we look more closely at the v_4 absorption (the same considerations apply to v_3, but the latter is more compact and the details less clear). The v_4 absorption is the result of a transition from the ground state to the first excited state of the v_4 vibrational mode (frequently designated $0 \rightarrow v_4$). Instead of a single line, however, in Fig. 4a we observe a considerable number of absorption grouped into three main branches labeled *P*, *Q*, and *R*. As pointed out earlier, this structure is primarily due to small rotational energy changes that accompany the main vibrational energy transition.

As depicted in Fig. 5, rotational energy levels *(J)* are closely spaced compared to vibrational energy levels *(n)*. Thus, a collection of molecules at room temperature will be found mainly in the lowest vibrational energy level ($n = O$) but will be distributed among a large number of rotational energy levels. Since the rotational energy for a given angular momentum is inversely proportional to the molecular moment of inertia, the heavier the molecule, the closer the rotational energy spacings. As a result, at room temperature the light hydrogen fluoride molecule significantly populates the lowest 10 or so rotational levels, but the heavier SF_6 molecule populates over 100 levels. This helps explain the abundance of absorption lines in the spectrum.

A transition between rotational-vibrational energy levels is induced by a coupling of the photon's electric field with the molecule's oscillating electric dipole moment. Quantum-mechanical arguments for the harmonic oscillator show that the selection rules for such changes of energy allow only transitions with $\Delta n = \pm 1$ and $\Delta J = -1, 0, 1$. The selection rules for ΔJ correspond, respectively, to the grouping of absorption into *P*, Q, and *R* branches. In Fig. 4a the spectrum is well enough resolved that the individual rotational-vibrational transitions of the *P* and *R* branches are apparent. Because there is no change in rotational angular momentum for the Q-branch transitions, the many transitions here tend to be superimposed.

Adjacent to the Q branch in v_4 are several

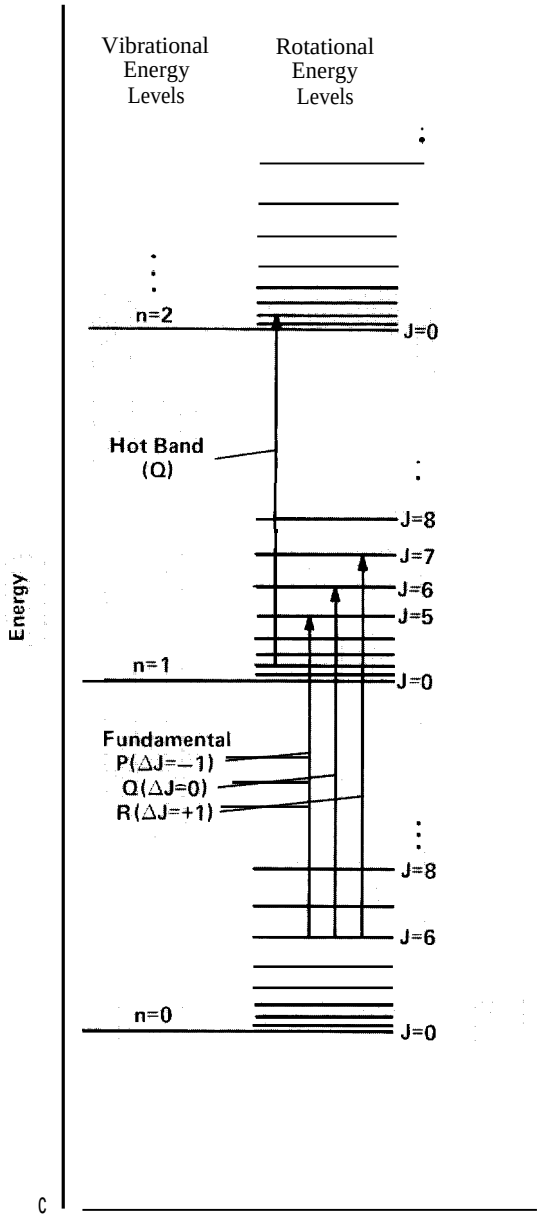

Fig. 5. Rotational-vibrational energy transitions. For a harmonic normal-mode vibration, the energy levels are equally spaced; these are represented here by the quantum number n ***with only the three lowest levels shown. The ground vibrational energy level*** (n = O) ***is not at zero energy because the Heisenberg uncertainty principle requires an oscillator never to be completely at rest. The rotational energy levels are represented by the total angular momentum quantum number*** J ***and have spacings that increase quadratically with*** J. ***Thus the frequency of a given energy transition depends on both the*** J ***of the starting level and the simultaneous change in rotational energy. Examples of allowed transitions out of the vibrational ground state*** (n = 0) ***are shown. The conventional designation is*** P(J), Q(J), ***or*** R(J), ***depending on the value of*** △J, ***plus the value of*** J ***in the lower state; thus, the three transitions shown are P(6), Q(6), and R(6). A single hot-band transition from*** n = 1 ***to*** n = ***2, Q(2), is also shown. The relative spacings of the rotational and vibrational energy levels will depend on the bond strengths and the molecular moments of inertia; typically, the rotational energy levels are much more closely spaced than depicted here.***

weaker absorption called hot bands. These absorption are due to v_4 transitions. but originate from an excited vibrational state instead of from the ground state (Fig. 5). The lower excited state either can be v_4 ($v_4 \rightarrow 2v_4$ rather than $0 \rightarrow v_4$) or can be another vibrational state ($v_i \rightarrow v_i + v_4$). These transitions are seen because they differ slightly in frequency from the central Q branch of the fundamental; in fact, they generally occur at lower frequencies. This happens because the vibration is not strictly harmonic. That is, as the bond is stretched further and further, the restoring force does not remain proportional to displacement and higher order enharmonic terms become important. These higher-order terms gradually decrease the equally spaced energy levels of a harmonic oscillator. When the originating states of hot bands can be identified, they provide useful information on the extent of anharmonicity in the vibration. In v_3 (Fig. 1) the hot-band structure largely obscures the *P* branch.

Single rotational-vibrational transitions can be further resolved with diode spectroscopy. This is shown in Fig. 4b for the *P(88)* transition which corresponds to the absorption of one quantum of v_4 vibrational excitation accompanied by a change in the rotational quantum number from $J = 88$ to $J = 87$ (that is, $\Delta J = -1$). Obviously *P*(88) is not a single line: at Doppler-limited resolution it displays the detailed structure shown. Even these features, however, consist of discrete clusters of transitions that yield to saturation spectroscopy as shown in Fig. 4c.

These coded messages about the interaction of the molecule with incident photons might seem to be particularly complicated for such a molecule as SF_6. However, the intricate spectra contain rather striking patterns that can be deciphered relatively easily. The simplicity that emerges may help us to understand complex high quantum states in general.

Spectral Clusters— Cracking a High Quantum Code

Why is the *P* (88) transition a collection of absorption of different frequencies rather than a single line at one frequency? Basically there is a distinction between rotations caused by the anisotropy of the molecule. If the properties of the molecule were spherically symmetric as depicted in Fig. 6, there would be only one absorption peak for *P(88)* because the molecule would be distorted in the same way regardless of the orientation of the axis of rotation. However, SF_6 molecules are octahedrally, not spherically, symmetric, and rotations about differently oriented axes produce different distortions in the molecule. These distortions correspond to different rotational energies and consequently to slightly different absorption frequencies.

The orientation of the rotation axis with respect to the symmetry axes of the molecule is the key to understanding the patterns of absorption peaks observed in the spectrum of molecules at high *J* values. But this classical consideration was not appreciated until after the spectrum was unraveled by a more laborious analysis of the quantum-mechanical Hamiltonian for the molecule. After presenting the quantum approach to this problem, we will show how the classical picture gives intuitive insight into the origin of the many lines in the *P(88)* spectrum.

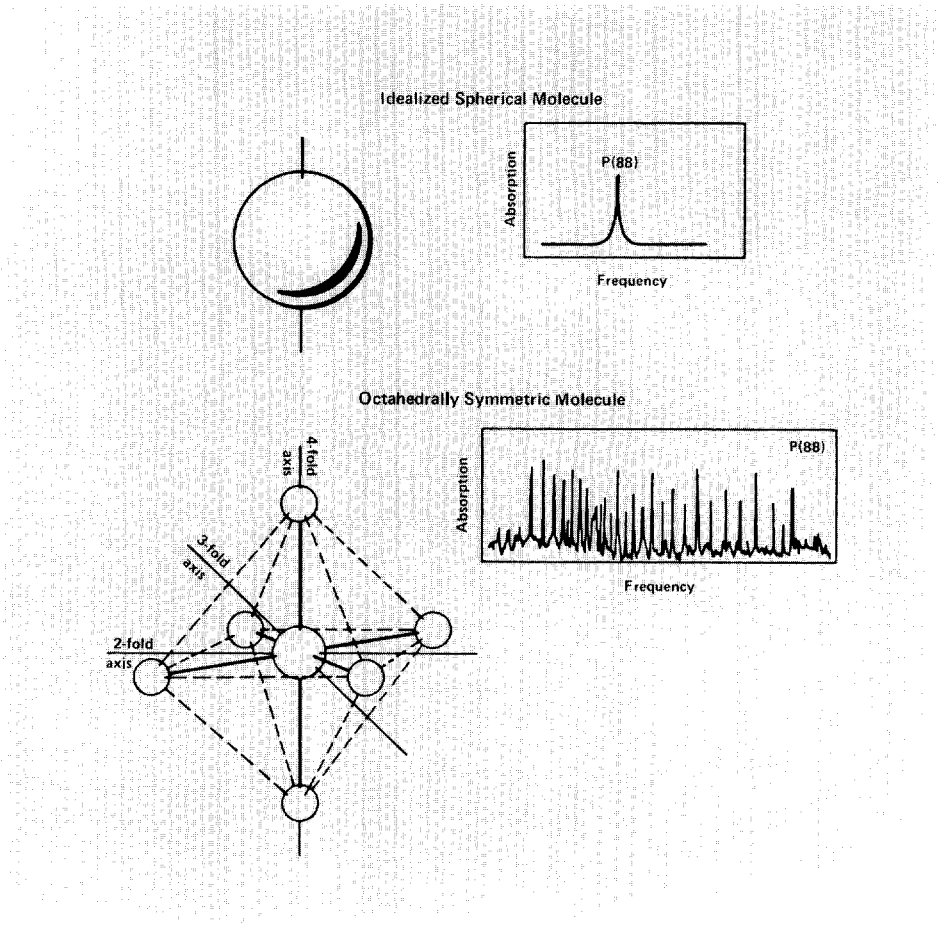

Fig. 6. ***The effect of molecular symmetry on the absorption spectrum of a rotational- vibrational transition. With a spherically symmetric molecule, all rotational axis orientations are equivalent, so there is only one absorption peak for a given rotational state (here J = 88). However, the SF_6 molecule is octahedrally symmetric, so different orientations of the rotation axis result in distinct energies, producing the complexity of the* P(88) *absorption band. Examples of axes with 4-fold, 3-fold, and 2-fold symmetry properties are shown; for instance, when the molecule rotates in increments of 3600/4 = 90° about the 4-fold axis, it arrives at positions that are indistinguishable from its starting position.***

QUANTUM APPROACH. As we mentioned earlier, the simplest model (or, in mathematical terms, the zeroth-order Hamiltonian H_o) of a molecule is a rigid rotor plus a harmonic oscillator. In order to describe the Coriolis forces experienced by the atoms in a rotating molecule, another term H_1 must be added to the Hamiltonian. H_1 has a very simple form if the molecule is described in a special coordinate system that is fixed in the body of the molecule. In this reference frame the molecule can be described in terms of its angular momentum *J* and the normal-mode coordinates corresponding to the molecule's independent vibrational motions. So far the Hamiltonian $H = H_o + H_1$ contains only scalar terms, that is, terms with spherical symmetry. The scalar nature of these terms dictates that a given rotational-vibrational energy level is shifted in energy but not split into different energy components. As a result, this first-order perturbation theory predicts a single absorption frequency for a given *J*.

In order to account for the observed energy splittings of the rotational states, the Hamiltonian must include second-order octahedrally invariant tensor terms reflecting the symmetry of the molecule ($H = H_o + H_1 + H_2 = H_{scalar} + H_{tensor}$). These tensor terms predict the detailed splitting of each rotational energy level into states at different energies with each state possessing a symmetry compatible with the overall octahedral symmetry of the molecule.

This type of Hamiltonian analysis has been used to identify all the details of complex spectral patterns of high-symmetry molecules. The Hamiltonian predicts relative spacings between energy levels and between absorption peaks. The overall multiplicative constants in the Hamiltonian that determine the size of the spacings are determined by examining the spectra,

Historically, the symmetries of the states into which the rotational levels split were determined by symmetry group analysis in a manner similar to that used by crystal spectroscopists in what is called crystal field theory. According to crystal field theory the various quantum orbitals of an atom located in the anisotropic electrostatic field of a crystal are distorted by that field in a manner determined by the relative orientation of field and orbitals. The consequent shifting of energy levels is called crystal field splitting, and the application of symmetry group analysis allows the number of shifted levels and their relative energy displacements to be identified and labeled.

For example, in crystal systems with cubic, tetrahedral, and octahedral symmetry, the labels for the atomic orbitals are A_1,A_2, E, T_1, and T_2. These labels describe the symmetry character of the orbitals distorted by the crystal field. An atomic s orbital, which has angular momentum $J = 0$, is labeled as a singlet A_1 state. An atomic p orbital, which has angular momentum $J = 1$, is a triplet T_1 state in the crystal field. This triplet state' remains degenerate or unsplit in the crystal field, although in the presence of an electric field it splits into three different states corresponding to different orientations of the angular momentum vector relative to the electric field. These orientations are given by the magnetic quantum numbers $m = 1$, 0, and —1. An atomic d orbital ($J = 2$) has five degenerate states of magnetic quantum numbers $m = 2$, 1, 0, –1, and –2, which in a cubic crystal field are split into two states, a T_2 (triplet) and an E (doublet). One can represent this energy splitting by the equation

$$d\ (J = 2) = T_2 + E\ .$$

A_2 also labels singlet orbitals, but it appears for the first time in the splitting of an f orbital or $J = 3$ septet:

$$f(J = 3) = A_2 + T_2 + T_1\ .$$

For the SF_6 molecule, instead of treating external electrostatic fields, the molecular physicist tries to model the effects of the internal electric field on the dynamics of the molecule. But the octahedral symmetry of the SF_6 molecule means that the same formulas used in crystal field theory to derive splitting equations in octahedrally symmetric fields are also applicable to SF_6. For an angular momentum state with $J = 88$, one can derive the splitting equation

$$X(J = 88) = 8A_1 + 7A_2 + 15E + 22T_1 + 22T_2\ . \qquad (1)$$

Thus the $J = 88$ state is split into 74 octahedrally symmetric states. If one takes into account that A_1 and A_2 are singlets, E is a doublet and T_1 and T_2 are triplets, then Eq. 1 accounts for all $2J + 1 = 177$ rotational quantum levels associated with this large (J= 88) angular momentum.

Since the ground vibrational state has negligible rotational splitting, the splitting observed in the spectrum is essentially that of the excited state. Thus one expects to see one absorption peak for each of the 74 states defined by Eq. 1. In the spectrum of Fig. 4b only about 26 lines are discernible, but in Fig. 4c we see that each of these actually corresponds to a cluster of two to four individual transitions. The clusters consist of the following combinations of symmetry species: A_1T_1E, A_2T_2E, T_1T_2, $A_1T_1T_2A_2$, and T_1ET_2.

The clustering of octahedral states and the identity of these states were predicted by diagonalizing the largest term H_2* in the second order Hamiltonian, namely the molecular "crystal field potential," or centrifugal distortion potential. This term can be written as

$$H_2^* \propto J_x^4 + J_z^4 + J_y^4 - (3/5)J^4\ , \qquad (2)$$

where J_x, J_y, and J_z designate the components of total angular momentum along the orthogonal S-F bond axes. A surface representing this potential is shown in Fig. 7a, and the classical physics of the potential will be described below. For now, it is important simply to note that the eigenvalues determined by diagonalizing this approximate H_2 for $J = 88$ predict the exact clustering and level spacing observed in the $SF_6\nu_4$ spectrum. This procedure leads to the correct assignments not only for the $SF_6\nu_4$ spectrum but for the rotational substructure for any J in any heavy high-symmetry molecule. Unfortunately, solution or diagonalization of the Hamiltonian to find the energy eigenvalues and rotational substructure requires time-consuming and expensive numerical calculations.

An additional clue to the correct assignment of the rotational substructure of Fig. 4b is provided by the relative intensities of the absorption. This clue was very useful in both the Q branch of ν_0 and the entire ν_1 band where absorption peaks associated with different J values overlapped. The assignments are made by matching the relative intensities of the absorption peaks with the relative intensities for each cluster predicted from nuclear spin statistics.

The relative intensities of absorption for the different species depend upon the number of nuclear spin states belonging to each species. This number is found by using the Pauli exclusion principle, which requires the total wave function, which includes nuclear spin, to change sign whenever two identical particles are exchanged. This principle is better known by its application to electronic spin-orbit structure in atoms or to symmetry species of diatonic molecules, For example, the existence of two nuclear-spin isomers of hydrogen (H_2) is well known. Here each nucleus is a proton with a nuclear spin of 1/2 in units of $h/2\pi$; that is, they are fermions with one-half quantum of intrinsic angular momentum. The spins can be aligned parallel ($\uparrow\uparrow$) or antiparallel ($\downarrow\uparrow$); the former results in "ortho" molecules with a unit-spin ($S = 1$) triplet of nuclear-spin states, the latter in "para" molecules with only a

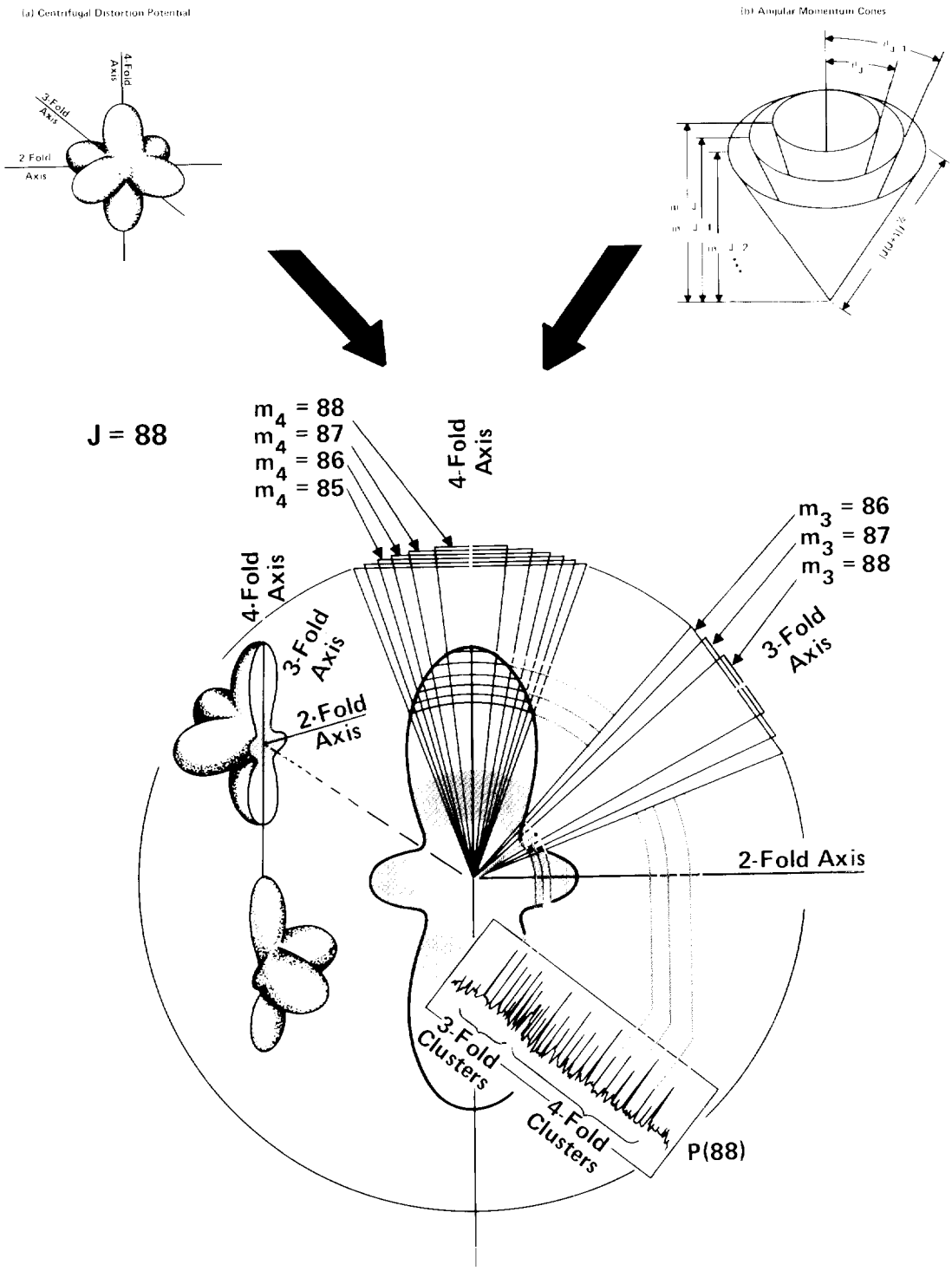

Fig. 7. Rotational axis clustering. (a) A plot of the appropriate centrifugal distortion potential arising from second-order perturbation theory for octahedrally symmetric molecules shows hilltops of maximum rotational energy around the 4-fold symmetry axes and valleys of minimum rotational energy around the 3-fold symmetry axes. There are saddle points at the 2-fold axes that only become obvious in the cross-sectional view of the surface in part (c). (b) Angular momentum cones are the allowed loci of angular momentum vectors for quantum states of magnitude **[J(J+1)]½** ***and azimuthal component*** m. (c) ***In this spectral nomogram for*** **P(88),** ***the intersections of the*** **J** ***=88 angular momentum cones with the potential surface approximately determine the spectra near maxima, minima, and saddle points on the symmetry axes. Note that as the cones around the 4-fold axis go to lower*** m_4 ***azimuthal quantum numbers, the absorption frequency decreases because the point of intersection is moving off the high-energy hilltop. However, for cones around the 3-fold axes, lower*** m_3, ***quantum numbers correspond to higher frequencies because the point of intersection is moving out of a low-energy valley.***

zero-spin ($S = 0$) singlet. Normal hydrogen thus consists of a 3:1 mixture of the ortho and para species. Consideration of the symmetry of the total wave function, together with the exclusion principle, allows these two to be matched with A_2 and A_1 symmetry species, respectively.

Similar effects will exist in any molecule composed of like nuclei with nonzero spins. The equivalent fluorine nuclei in SF_6 also have a nuclear spin of 1/2. The exclusion principle applied in this case allows the A_1 symmetry species to have only singlet states as in H_2, but in SF_6 there happen to be two A_1 species. The A_2 species in SF_6 have a spin triplet ($S = 1$) and also a septet ($S = 3$), or ten spin states in all. (Recently, the very highest resolution saturation spectra taken by C. J. Borde at the University of Paris showed evidence of ten sub-peaks in an A_2 absorption, each split about 10 kilohertz apart. This splitting is called hyperfine structure and is due mainly to spin-rotation interactions.) The spin-statistical weights for these and the remaining symmetry species of octahedral molecules were worked out at Los Alamos by H. W. Galbraith and C. D. Cantrell in 1974, and are 2:10:8:6:6 for the A_1: A_2: E:F_1: F_2 levels.

Examining the *P(88)* fine structure in Fig. 4b (using *W* for weak, *M* for medium, and *S* for strong relative intensities), we see that the main absorption peaks on the right side of the spectrum have a four-peak, repetitive pattern of intensities *MWSW,* which cycles somewhat more than four times. On the left side the three-peak pattern of *MSM* repeats at least two cycles. By relating the known statistical weights to the relative intensities in the spectra, each absorption can be labeled with the appropriate symmetry species cluster derived from Eq. 2. All 74 symmetry species predicted by Eq. 1 were accounted for in the *P* (88) manifold of the spectrum.

It is at this point, however, that the remarkable order in the spectrum becomes most apparent. The cyclic pattern of intensities revealed in the fine structure is based on a cyclic ordering of clusters. Thus, on the right in Fig. 4c, reading backwards, there is a cycling of the four clusters A_1T_1E, T_2T_1, ET_2A_2, T_2T_1 (weights 16, 12, 24, 12, respectively, or *MWSW),* and on the left, a cycling of the three clusters T_2ET_1, $A_1T_1T_2A_2$, and T_2ET_1 (weights 20, 24, 20, or *MSM).* One notices in other rotational-vibrational transitions the regularity of these same sequences repeated over and over. Moreover, a specific order is continued into the superfine structure; each type of cluster has an order and relative spacing of symmetry species within it. Unexplained clusterings of energy levels are sometimes called accidental degeneracies, but it is clear that the SF_6 cluster degeneracies have a meaning.

Hints of clustering have emerged in other theoretical works. Analyses of ion-crystal-field thermodynamics contained some similar clusters in numerical solutions. Computer studies of rare-earth electronic spectra by Lea, Leask, and Wolf in 1962 provided the first evidence of clustering in angular momentum levels. Computer solutions of methane by Dorney and Watson in 1972 provided the first examples of clusters in molecular theory. But it was the spectral scans over a wide range of frequencies made available by tunable lasers at Los Alamos starting in 1974 and the exhaustive computer analyses of the second-order Hamiltonian by Galbraith, Krohn, Louck, and others that finally revealed the full extent and regularity of cluster patterns. However, the reason behind the remarkable regularity of the cluster patterns remained a mystery.

A CLASSICAL APPROACH. The physical origin of the cluster patterns was not understood until a classical, though approximate, approach to the problem was taken. This approach developed from a closer look at the possible orientations of the rotational axis for a given *J* relative to the symmetry axes of the molecule and the relationship of that orientation to centrifugal distortion of the rotating molecule.

Centrifugal distortion always increases the moment of inertia and therefore decreases the rotational energy for a given *J.* An octahedral SF_6 molecule has the least centrifugal distortion and thus the highest rotational energy for a given *J* when rotating around its fourfold symmetry axes, for these axes are along or perpendicular to its strong radial sulfur-fluorine bonds (Fig. 6). The rotational energy decreases if the rotation axis is along a twofold symmetry axis because then centrifugal force tends to bend four of the radial bonds, which is easier than stretching them. The molecule suffers the most distortion and therefore has the lowest rotational energy for a given *J* when rotating on its threefold symmetry axes, which lie exactly betwen radial bonds, thus allowing all six bonds to bend.

This can be seen if one uses the centrifugal distortion potential of the second-order Hamiltonian (Eq. 2) and plots this part of the SF_6 rotational energy radially on a globe. One finds hilltops, or local maxima, around the fourfold symmetry axes and valley bottoms, or local minima, around the threefold axes (Fig. 7a). The importance of this plot is that for a selected orientation of the axis of rotation one can judge the relative shift in the rotational energy due to centrifugal distortion and, thus, the corresponding relative shift in the absorption frequency.

But what orientations are allowed? The elementary quantum theory of angular momentum describes the allowed orientations of the rotational axis for an orbital state of angular momentum *J.* It states that the angular momentum vector has a length of $[J(J+1)]^{1/2}$ and that the z-component of the vector equals the azimuthal quantum number *m,* where *m* can assume values in integral jumps from *J* to —*J.* In other words, the *J* vector is constrained to lie on a cone of altitude *m* and slant length $[J(J+1)]^{1/2}$ (Fig. 7b). These cones can then be used to locate possible orientations of the axis of rotation with respect to the SF_6 rotational energy surface.

Which cones most closely approximate the cluster patterns? Figure 7C is a nomogram showing the select group of $J = 88$ angular momentum cones that generates the *P* (88) absorption of Fig. 4a. One sees that the high-frequency portion of the spectrum is associated with angular momentum cones intersecting the energy surface close to the fourfold-axis hilltops. Evidently the highest-m states ($m_4 = 88, 87, 86 \ldots$) are preferred; these are "low-uncertainty" states with the narrowest cones and the smallest uncertainty in transverse (*x* and *y)* components of momentum. The low-frequency portion of the *P* (88) spectrum corresponds to similar low-uncertainty cones localized around threefold axes. The boundary between these regions contains a few disordered spectral lines. From Fig. 7C it is evident that these are associated with saddle points at the twofold symmetry axes. An angular momentum vector cannot be localized stably around these points; it is free to thread its way all around the globe, going from one saddle point to the next without changing its energy. When this happens, the molecule tumbles wildly like a diver doing uncontrolled gainers. Thus, the appropriate orientations of the rotational axes that account for almost the entire spectrum are those that have a high z-component of angular momentum along a fourfold or

threefold symmetry axis.

For many molecular states, including the S F_b fundamental vibrational modes, the angular momentum nomograms are a useful alternative to expensive numerical solutions of the detailed Hamiltonian. Computer diagonalization of the Hamiltonian may bog down for angular momenta quanta that range into the hundreds, but the analytic approximations needed to generate the nomogram generally improve with higher quantum numbers. We might say that the analytic results inject a bit of classical common sense into an otherwise difficult quantum problem.

Patterns Within the Clusters

We now have some physical insight concerning the pattern of clusters, As already noted, there is further splitting and order within clusters, again predicted by the second-order Hamiltonian, However, a more classical approach is needed to achieve physical insight concerning this superfine splitting.

All clusters associated with the fourfold axes *(TT* or *ATE)* have six states; for example, the first A_1T_1E cluster on the right of Fig. 4C is made up of a singlet, a triplet, and a doublet—six states in all. This agrees with the fact that a given angular momentum cone can be oriented either up or down about any of three fourfold axes resulting in six equivalent states for each rn_4 quantum number. The same reasoning applies to the clusters associated with threefold axes *(TET* or *ATTA):* each cluster has eight states and there are eight equivalent orientations about the four threefold axes for each rn_3 quantum number.

But we know from saturation spectroscopy and the Hamiltonian analysis that the states within the clusters are not equivalent, Apparently, the rotational-energy-surface approach in which the orientation of the *J* axis remains fixed does not take fully into account the octahedral symmetry of the molecule. The additional effect that remedies this incomplete treatment, and that finally breaks the symmetry of the clusters into separate absorption for each octahedrally invariant symmetry species, involves an interesting interplay between classical and quantum behavior.

ROTATIONAL TUNNELING, Briefly, tunneling of the rotational axis between apparently equivalent states causes the splitting. For example, the A_1T_1E cluster of *P* (88) in Fig, 4C with $m_4 = 76$ is a cluster with its momentum localized around a fourfold symmetry axis at a hilltop. However, there are six such hilltops, one for each of the directions north, south, east, west, up, and down (Fig, 7a). Quantum theory allows a momentum vector or rotation axis to tunnel from one hilltop to another, which is not permitted in classical mechanics, Quantum tunneling can be understood to occur through resonance between equivalent states and can be expected between any states with the same or nearly the same energy.

It turns out that the tunneling effect is usually quite small and involves hilltops that are nearest neighbors only. For example, the up hilltop has a tunneling rate S with the east, north, west, and south hilltops because those hills surround it. The up-to-down tunneling amplitude, however, is nearly zero since these hills are too distant for appreciable tunneling,

One can find resonant combinations of the six hill states (called stationary states or eigenstates) whose energies are unchanged by the resonant action of nearest-neighbor tunneling. The first such state is an equal sum of all six hill states, so it is labeled by the singlet A_1 symmetry species (Fig. 8). If the classically expected value of a hilltop angular momentum state is *H,* then the A_1 singlet has an energy *(H - 4S)* which is the classical value minus the effect of tunneling to the four nearest neighbors, The next three degenerate eigenstates are differences between antipodal hill states, for example, up minus down, and they are labeled by the triplet T_1 symmetry species. All three have the same energy (H) since there is no tunneling in this combination. Finally, there is a pair of *E* states, with the energy *(H* + 2S) needed to conserve total energy for the cluster.

In this way one can decipher the intracluster structures. If one resolves an A_1T_1E grouping, three lines will appear with a T_1 line between the A_1 and *E* lines. The spacing should be 4 *S* between A_1 and T_1 and exactly half this much between T_1 and *E*. This two-to-one ratio of spacing has been seen in virtually all A_1T_1E and A_2T_2E clusters that have been resolved in laser spectra. Similarly, the threefold clusters $A_1T_1T_2A_2$ and T_1ET_2 can be analyzed; one finds that their component lines are all equidistant. This is observed easily and with great precision in computer experiments, which can be as illuminating as those done in the spectroscopy laboratory.

In fact, some of the intracluster splittings due to rotational-axis tunneling will not be resolvable by any spectroscopic techniques. Figure 4C shows that the estimated values of many cluster splittings are so tiny that they will probably never be seen directly. The splitting of the fourfold clusters range from 2 X 10^{-4} to 2 X 10^{-22} cm-l, the latter corresponding to a frequency of about one cycle in 50 centuries! The splittings are proportional to the axis tunneling rates S, or the rate at which the molecule may tumble in the absence of other perturbations. It is interesting to note that the smallest splittings are at the two ends of the *P* (88) spectrum (Fig. 4c), that is for states with high m_4 or high m_3 in which the rotation axis is most localized. As the orientation of the axis moves away from either the fourfold or the threefold axis and toward the unstable saddle point region between, the splitting, and therefore the tumbling, of the molecule increases as expected.

However, whenever the energies of different states come arbitrarily close together, one should expect even small perturbations to have large effects. Most of the clusters in Fig. 4C have intracluster splittings due to axis tunneling that are less than 20 kilohertz, and this is comparable to or less than what is expected for the next level of splittings; the intra-species, or hyperfine, splitting. Normally, one would not expect nuclear spin-rotation perturbations to be large enough to have much influence, and the

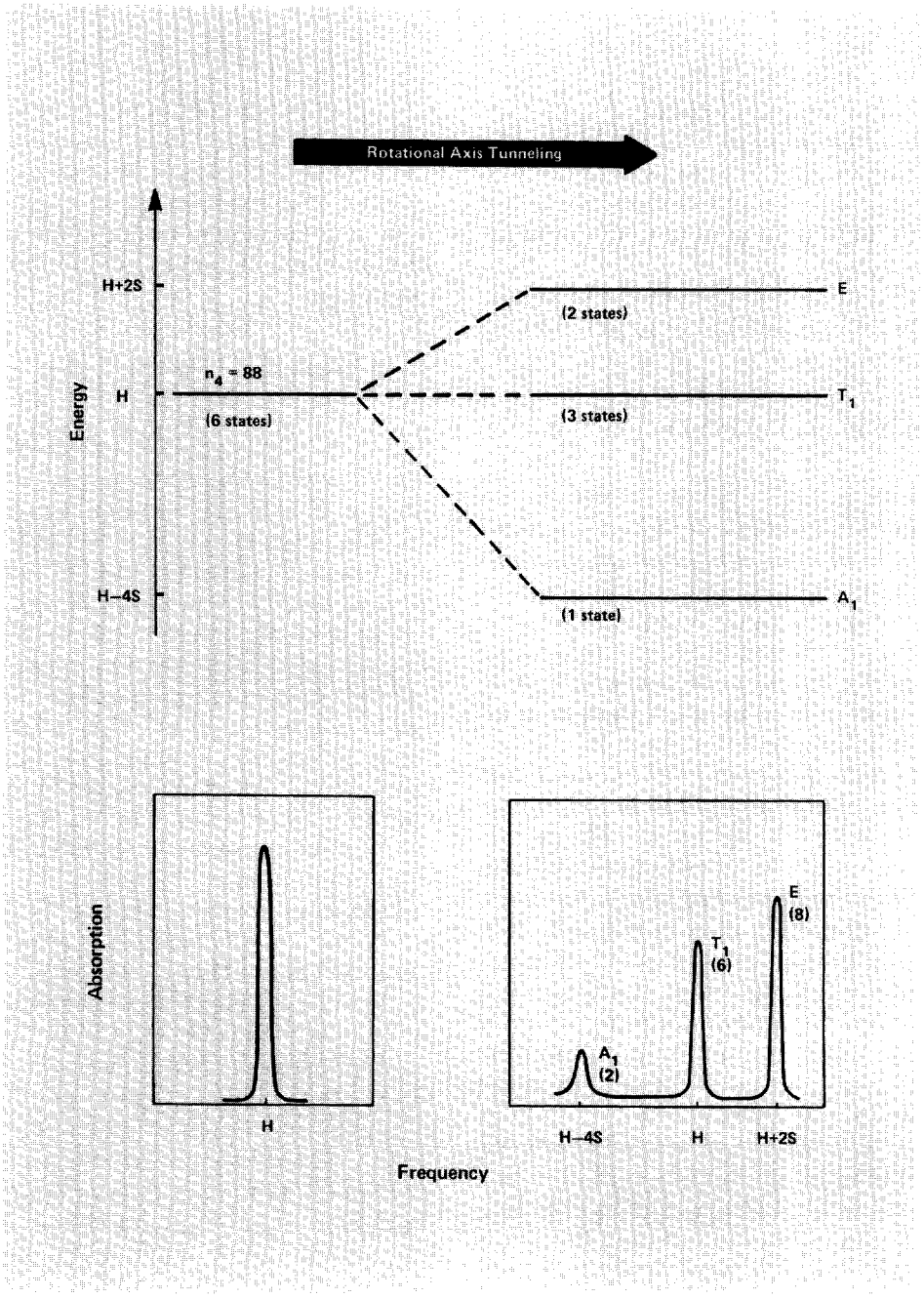

Fig. 8. Superfine structure. The effect of quantum mechanical tunneling between equivalent nearest-neighbor rotational-axis orientations is illustrated for an A_1T_1E ***4-fold axis cluster in*** P ***(88). The mixing of the 6 possible*** m_4 ***= 88 states results in one state reduced in energy by 4 times the tunneling rate (H – 4S) and 2 states increased in energy by 2 times the rate (H + 2S). In the absorption spectrum this corresponds to a distinctive 2-to-I spacing of the peaks. When the relative heights of the*** A_1, T_1, E ***peaks (the corresponding nuclear-spin statistical weights are shown in parentheses) are also taken into account, the*** A_1T_1E ***cluster is easily identifiable.***

usual picture is of nuclear spin vectors riding like Ferris-wheel cars around a tumbling molecule. However, the clustering allows the nuclear spin precessional motion to be in resonance with the rotational motion, or for the spins to act in some ways like tiny gyrostabilizers that further retard tumbling. In essence, there must be a strong mixing between individual spin species and their spin multiplets so that A_1, A_2, E, F_1, and F_2 are, by themselves, no longer good labels of molecular states. This is very different from the usual situation in, say, hydrogen, where ortho and para species are like separate compounds. Research on the unexpected hyperfine effects associated with the small superfine splittings is still under way.

Molecular Constants

We now have some understanding of the origins of the complex rotational structure observed in the vibrational spectra of high-symmetry molecules. These considerations allow the spectroscopist to assign each absorption feature to a transition between specific quantized rotational-vibrational levels. If these assignments are used to fit a frequency expression derived from the appropriate Hamiltonian, then various molecular constants can be determined that measure the importance of each of the various effects.

To see how this is done, first consider the rotational absorption in the *P* and *R* branches. To simplify the discussion, we deal only with the scalar approximation, in which *P* (88), for example, would appear as a single peak.

The "line" positions are given by a polynomial in the total angular momentum quantum number *J*, which includes both normal rotational and vibrational angular momentum. For the *R* branch, the frequency expression, somewhat simplified, is

$$\nu_R(J) = \nu_0 + 2B(1 - \zeta)(J + 1) + \Delta B(J + 1)^2 - 4D(J + 1)^3 + \ldots . \quad (3)$$

The same equation holds for the *P* branch if $(J + 1)$ is replaced by $(-J)$.

The constants in Eq. 3 have the following significance. The first, ν_0, represents the band origin (that is, the frequency of the transition in a hypothetical nonrotating molecule). The constant *B* is the mean rotational constant of the two vibrational states involved in the transition and is inversely proportional to the mean molecular moment of inertia. The Coriolis constant ζ measures the amount of vibrational angular momentum in the normal mode (this effect will be treated more fully in the next section). The approximate difference ΔB between the rotational constants in the lower and upper states accounts for the change in the moment of inertia when the molecule is excited vibrationally. Finally, *D is* a centrifugal distortion constant. To give an idea of the magnitudes involved for ν_4 of SF_6 these parameters in cm–' are

$\nu_0 = 615.020,$
$B(1 - \zeta) = 0.1108,$
$\Delta B = -1.96 \times 10^{-5},$
and
$D = 1.3 \times 10^{-8}.$

The *P* and *R* absorption peaks of Fig. 4a are thus spaced by approximately $2B(1 - \zeta)$ = 0.222 cm-l and their assignment is simply a matter of counting. For ν_3 of SF_6, on the other hand, the manifolds are much closer since $B(1 - \zeta) = 0.0279$ cm^{-1}. This smaller separation is accompanied by larger tensor splittings in the ν_3 vibration so that the various component peaks overlap much more. As a result, isolated absorption such as *P* (88) cannot be observed in ν_3, and this explains the more compact nature of this band. The assignments can still be made, though the process is considerably more tedious.

After the assignments are complete, the energy level expression, including both the scalar part discussed above and tensor terms to describe splitting, is fitted to the data by a least-mean-squares procedure. The spectroscopic constants that result from this analysis specify the frequency of any given rotational-vibrational transition and provide an insight into the dynamics of the molecular motion.

In the Q branch the absorption frequencies, to the same scalar approximation, are given by

$$\nu_Q(J) = \nu_0 + \Delta B' J(J + 1) + \ldots \quad (4)$$

Here $\Delta B'$ is a constant similar but not identical to ΔB (in ν_4 of SF_6, $\Delta B' = 0.97\,\Delta B$ = –1.91 x 1O^{-5} cm-l). Note that there is no $B(1 - \zeta)$ term since the *Q* branch represents transitions with no change in rotational angular momentum energy. As a result, spacing between J-transition peaks in the *Q* branch is obviously much less than in the other branches, and in fact is less than the rotational-anisotropy splitting of each transition, even for small *J*. The resulting overlap accounts for the sharpness of the *Q* branch, and it makes assignments extremely difficult. In Fig. 2c, for example, the absorption seen correspond to transitions arising from $J = 34$ to *J* values in the nineties, even for this short portion of the *Q* branch. However, various techniques, including computer synthesis of the branch contours, have enabled spectroscopists to make detailed assignments even in such difficult regions.

The precision with which the molecular parameters can be determined by these methods is remarkable. If the measurements are made with tunable diode lasers over a wide frequency range, the data set may consist of many hundreds of lines, which helps to insure a fit that is mathematically "robust" and resistant to possible errors in a few of the points. Saturation data typically consist of fewer lines, but the frequencies of these can be determined with precision of the order of 10^{-7} cm-l. In fitting an "isolated" band-one not significantly perturbed by interactions with nearby energy levels—a lower-order spectroscopic parameter such as the band origin, ν_0, might be obtained with an uncertainty approaching that attached to the fundamental physical constants themselves. Results of this precision were beyond the reach of infrared techniques until the development of laser spectroscopy.

The Multiphoton Ladder

Up to this point we have been concerned with vibrational fundamentals, in which the transition is from the vibrational ground state to a singly excited upper vibrational level. Because of the electrical and mechanical anharmonicity of the vibrations, however, combination, difference, and overtone frequencies will also appear in the vibrational spectrum, though with greatly reduced intensities compared with the fundamentals. The hot bands and the overtones ($0 \rightarrow 2\nu_3$, $0 \rightarrow 3\nu_3$, etc.) are of special importance because they give information on the higher vibrational levels, which are very important in laser photochemistry.

When heavy symmetric molecules, such as UF_6, SiF_4, and SF_6, are irradiated using a high-power infrared laser coincident with a certain strong absorption feature, they can be vibrationally excited to the point of dissociation. In the case of SF_6 the dissociation occurs after the molecule absorbs some 30 infrared photons, whereas for UF_6 some 40 photons are required. The multiple-photon absorption of these and other molecules has fascinated chemists who are interested in bond-selective laser chemistry or in laser isotope separation.

Using a simple picture of the overtone levels of a spherical-top molecule, one might conclude that multiple-photon absorption is impossible. The first few energy levels, symbolized by $(n\nu_i)$, of a one-dimensional oscillator, such as the stretching mode ν_i of a linear molecule, are given by

$$(n\nu_i) = n(\nu_0) + X_{ii} n(n - 1) \ . \quad (5)$$

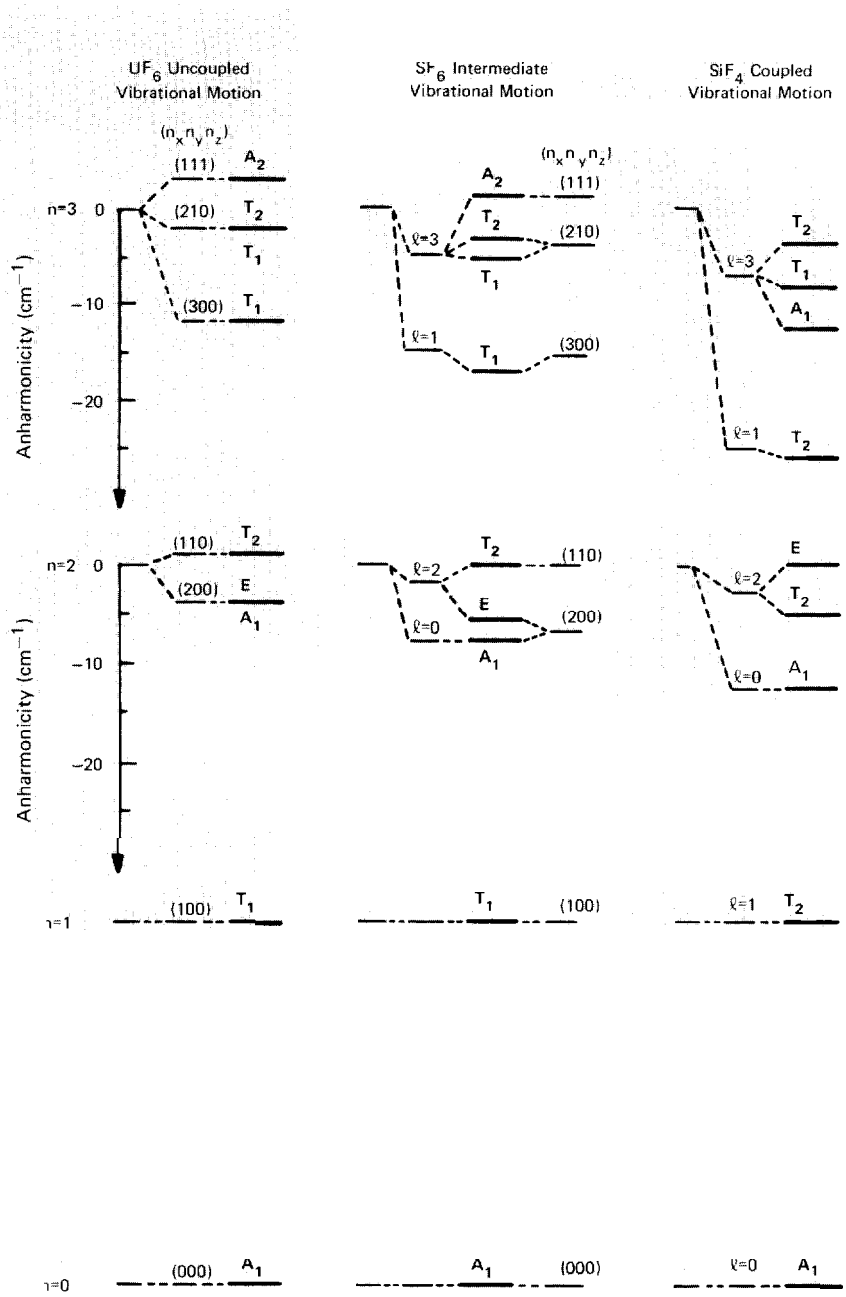

Fig. 9. The lower levels of the nv_3 vibrational ladders of UF_6, SF_6, and SiF_4, showing the effects of anharmonicity and splitting. Because the three degenerate v_3 components are strongly coupled in SiF_4, vibrational angular momentum is important and the quantum number l is used to label the major energy-level splittings. At the opposite extreme, the large UF_6 molecule has uncoupled vibrational motion and the major energy level splittings are best described with separate quantum number n_x, n_y, and n_z, for each of the three orthogonal motions. SF, is intermediate and must be dealt with as a mixture of both types of motion. The final energy states, after all splitting effects are accounted for, are labeled with their appropriate symmetry species.

Note that here, as compared to Eqs. ***3*** and 4, the terms representing rotational structure have been dropped for simplicity, the principal quantum number *n* is multipled by the band origin of the fundamental to represent the amount of vibrational excitation, and a scalar term has been added to account for the main shift in energy due to anharmonicities. The enharmonic coefficient X_{ii} is usually negative (X_{33} = –0.95, –1.7, and –2.9 cm^{-1} for the v_3 vibration of UF_6, SF_6, and SiF_4, respectively), which means that the energy levels are successively closer with increasing vibrational quanta. Thus for the *nth* photon absorbed, a laser emitting at frequency v_0, will be detuned by $X_{ii}n(n-1)$ above the resonant energy level of the molecule. When this detuning exceeds the effective laser linewidth, further absorption becomes difficult. The detuning will be reduced somewhat by the rotational structure of the molecule, but this is generally not enough. In fact. linear molecules are known not to absorb many photons even at high laser intensities, for just this reason.

This simple picture does not correctly describe polyatomic molecules because they are multidimensional oscillators and their higher vibrational energy levels ($n \geq 2$) exhibit splitting. This splitting is shown in Fig, 9 for the v_3 vibrations of UF_6, SF_6, and SiF_4.

The origin of the vibrational splitting lies, once again, in the fact that the various molecular motions are not independent. For example. with degenerate vibrations such as v_3 or v_4 the actual motion of the SF_6 molecule will be a combination with arbitrary phase of the degenerate modes. Each nucleus will thus move not in a linear fashion, but on the surface of an ellipsoid. These ellipsoidal motions introduce an angular momentum C to the vibration such that the molecule's total angular momentum *J* is a vector combination of the vibrational and pure rotational angular momentum. The concept of vibrational angular momentum is most readily illustrated by the degenerate

bending mode of a linear triatomic molecule such as $C0_2$ (Fig. 10a). This mode consists of two component vibrations that are strictly planar when viewed separately, but when they are combined with a 90° phase difference, the resulting motion has a rotational character that generates a vibrational angular momentum. The more complex combination of just two components of the v_3 stretching mode of SF_6 is depicted in Fig. 10b.

Because of such coupling phenomena as vibrational angular momentum, the splitting of the v_3 vibrational energy level needs to be represented by two tensor terms that account for anharmonicities of motion both along the bond and perpendicular to the bond. In SF_6 these anharmonicities correspond, respectively, to bonding interactions between the sulfur and fluorine atoms, and nonbonding interactions between two adjacent fluorine atoms. If these terms are added to Eq. 5, the energies for the nth overtone of v_3 may be adequately represented for $n < 5$ by

$$(nv_3) = n(v_0) + X_{33}n(n-1) + (G_{33} + 2T_{33})\ell^2 + T_{33}(10s - 8n - 6n^2) \ . \qquad (6)$$

The first tensor-splitting term, with the coefficient $(G_{33} + 2T_{33})$, is for nonbonding interactions and includes the vibrational angular momentum operator ℓ^2. The last term, with the coefficient T_{33}, includes both the enharmonic splitting operator s and the principal quantum number *n;* a dependence on *n* for this bonding-interaction term is not surprising since higher vibrational excitation leads to larger displacements along the bond and so to greater anharmonicities.

Again, because of the octahedral or tetrahedral symmetry of the UF_6, SF_6, and SiF_4 molecules, each vibrational level represented in the splitting belongs to one of the symmetry species A_1, A_2, E, T_1, or T_2. However, the directions and orders of shifting for these levels are seen to be quite

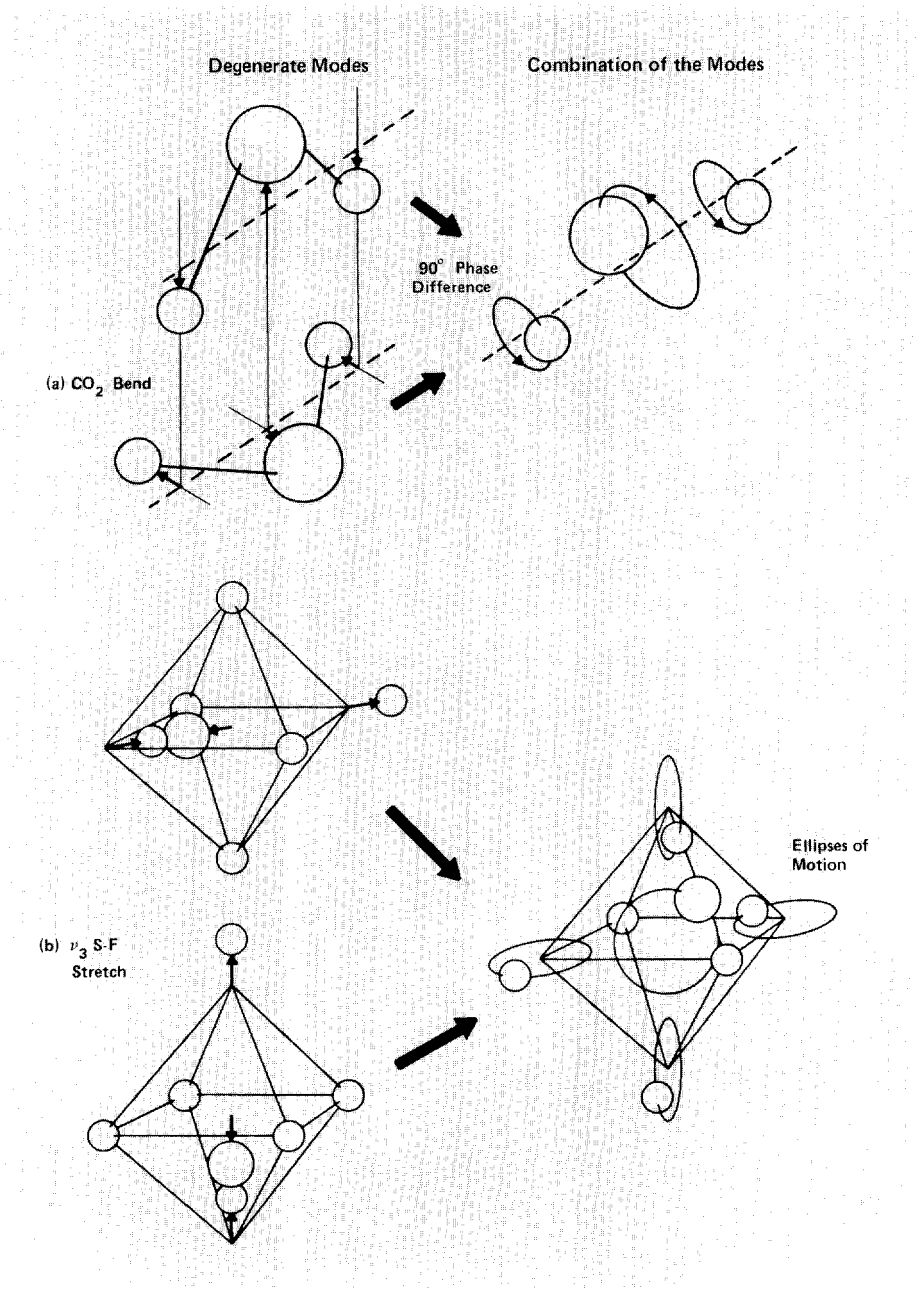

Fig. 10. Vibrational angular momentum. (a) If the two orthogonal components of the degenerate bending vibration of CO_2 are combined with a 90° phase difference, the bent molecule will generate vibrational angular momentum about the bond axis. (b) A similar but more complex situation exists for the degenerate vibrational modes of SF_6. Combination of the components of these modes with arbitrary phase will cause each nucleus to move on the surface of an ellipsoid. The 2-dimensional ellipses of motion that result from the combination of just two of the v_3 components are depicted (the widths of the four ellipses have been exaggerated for clarity). Vibrational angular momentum ℓ interacts with the angular momentum J of the molecule as a whole and is accounted for in the Hamiltonian with a $J \cdot \ell$ Coriolis force term and higher-order tensor terms.

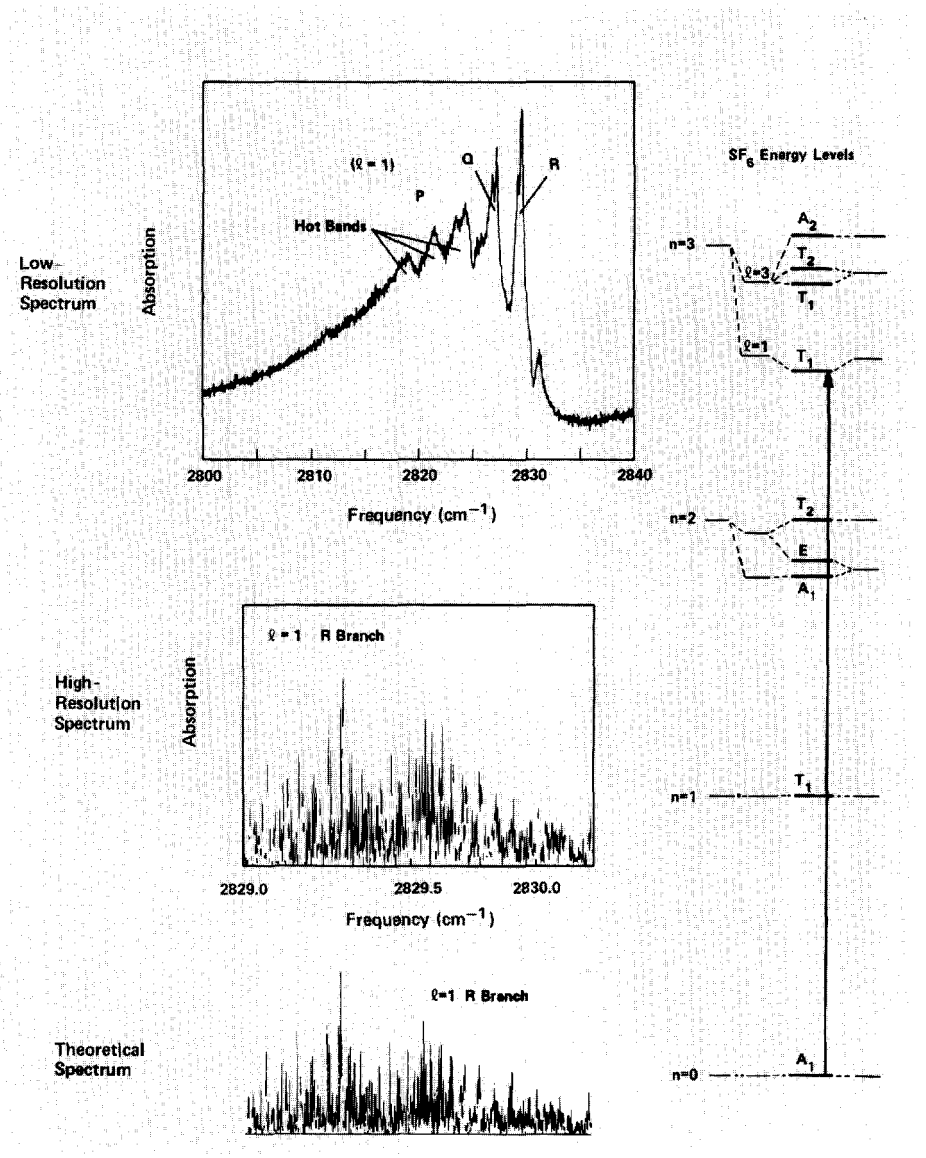

Fig. 11. The overtone $3\nu_3$ of SF_6. The upper spectrum was obtained with a Fourier-transform infrared interferometer at a resolution of 0.04 cm^{-1}. The middle spectrum is a Doppler-limited scan recorded by A. S. Pine at the MIT Lincoln Laboratory using a difference frequency spectrometer. It shows the rotational fine structure of the R branch of the $\ell = 1$ transition; the vibrational energy transition corresponding to this spectrum is shown on the energy level diagram at the right. The bottom panel illustrates the match that is possible with a theoretical simulation of the spectrum.

different for the three molecules depicted in Fig. 9. In fact, there is an opposite limiting behavior for SiF_4 and UF_6; SF_6 is intermediate between the two extremes. The reason for the differences lies in the relative importance of the two tensor splitting terms in Eq. 6.

For the case of SiF_4 we find, from analysis of the $3\nu_3$ spectrum, that $T_{33} << (G_{33} + 2T_{33})$. In this limit the ℓ^2 operator results in vibrational angular momentum values of the form $\ell(\ell + 1)$, where ℓ is the vibrational angular momentum quantum number. The allowed values of ℓ are $n, n-2, n-4, \ldots, 1$ or 0, and for SiF_4 ℓ is nearly a good quantum number. In other words, the major energy shifts for SiF_4 (labeled in Fig. 9 with ℓ) are due to the ℓ^2 operator. These levels lie at the center of gravity of the smaller shifts (labeled with the appropriate symmetry species) due to the s operator.

The physical significance of the dominance of the nonbonding interaction term for SiF_4 is that the three orthogonal motions of the degenerate ν_3 vibration are strongly coupled by the angular anharmonicity. This should be expected for SiF_4, which has a small, light central atom and crowded fluorine atoms that are able to "see" each other as they vibrate.

For UF_6 we find, again from analysis of the $3\nu_3$ spectrum, that $T_{33} >> (G_{33} + 2T_{33})$. In other words. bonding interactions dominate here. In this limit thes operator has values of the form $n_x^2 + n_y^2 + n_z^2$, where n_x, n_y, and n_z refer to uncoupled motions in the three perpendicular directions. These three quantum numbers describe excitations of independent simple harmonic oscillators, and each assumes the values O, 1, 2, . . . Thus, in Fig. 9, the major energy shifts for UF_6 are labeled $(n_x\ n_y\ n_z)$ while the finer splittings due to the ℓ^2 operator are labeled with symmetry species labels.

Because of the independence of the oscillations in the three directions, the motions can be described as localized vibrational modes rather than as normal modes of the molecule as a whole. This "local mode" concept has been used extensively in treating certain molecules like benzene (C_6H_6) in which stretching motions of the C-H bonds behave as though each bond were isolated from the rest of the molecule. Although this does not strictly happen in UF_6, each of the three degenerate vibrations of the ν_3 mode does behave here as if it didn't see the other two. In fact, model calculations by B. J. Krohn have shown that when the nonbonding interactions are weak and the mass of the central atom is much larger than that of a fluorine atom (which is the case for UF_6), then the ratio G_{33}/T_{33} approaches -2 and the ℓ^2 term tends to zero.

The drastic difference in the structure of energy levels between SiF_4 and UF_6 also leads to different selection rules, or pathways, for multiple-photon absorption. Since SF_6 is in an intermediate region, it shares some of the characteristics of both SiF_4 and UF_6, and its pathways are the most complicated. In Fig. 9 the effect of its nonbonding interaction term is shown to the right, the effect of the bonding interaction term to the left, and the final energy levels in between.

It is clear from Fig. 9 that the enharmonic splitting of the ν_3 overtones partially compensates for the overall shift of levels to lower energy as discussed above, so that multiple-photon pathways become accessible. The rotational structure of the molecules further splits the levels and helps to minimize laser detunings.

As already mentioned, the enharmonic constants X_{33}, G_{33}, and T_{33} determining the $n\nu_3$ energy levels of Fig. 9 were derived from analyses of the rotational-vibrational levels of the $3\nu_3$ high-resolution spectra for each of the three molecules studied. Typical low- and high-resolution spectra are shown in Fig. 1 I for the $3\nu_3$ band for SF_6.

Only the $\ell = 1$ transitions of $3\nu_3$ are shown and, in fact, transitions to the three t' = 3 levels are weak for the three molecules studied. We were able to determine their positions primarily by their influence on the $\ell = 1$ rotational-vibrational levels.

In order to duplicate the complicated structure revealed in Fig. 11. we needed seven rotational-vibrational constants in addition to the three enharmonic constants. With these 10 constants we fitted over 700 lines of the $3\nu_3$ SF_6, spectrum with a standard deviation of 4 x 10^{-4} cm-'. In constrast, a much simpler ν_3 spectrum of CH_4 recently required over 60 constants to give a tit of 0.02 cm-'. Although the resolution necessary for heavy symmetric molecules causes experimentalists difficulties, such molecules are certainly much nicer for theoreticians!

Once the first few rungs of the ν_3 ladder

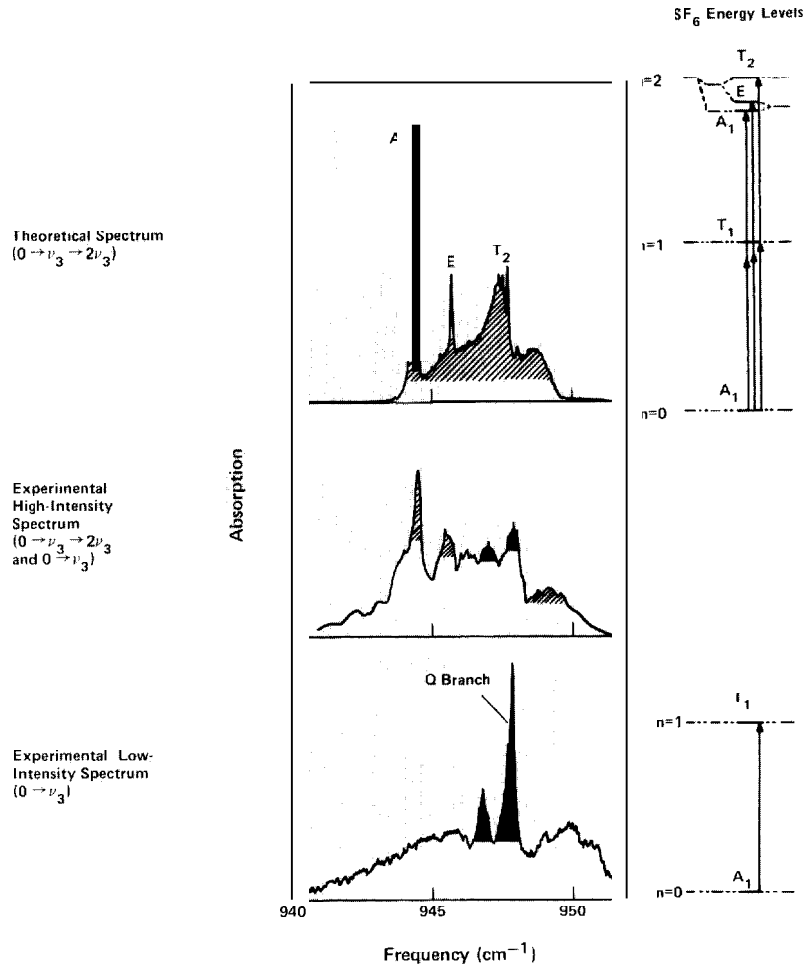

Fig. 12. Two-photon absorption. The lowest panel is a normal low-intensity absorption spectrum for the v, vibrational mode of SF_6 (similar to Fig. 2a, but recorded with fewer absorbing molecules), and thus represents single-photon transitions from the ground state **(n = 0)** ***to the first excited state*** (n = 1) as ***shown on the right. The high-intensity (3 megawatts per square centimeter) spectrum in the middle (observed by S. S. Alimpiev*** et al. ***at the Lebedev Physics Institute, Moscow) still has the single-photon peaks (black) and, in addition, has peaks that can be attributed to two-photon jumps between the*** n = O ***and*** n = ***2 levels (shaded). The theoretical shape of just the two-photon contribution to the spectrum, based on an analysis of $3\nu_3$, is shown at the top with the appropriate $0 \rightarrow \nu_3 \rightarrow 2\nu_3$ energy transitions to the right (shifts in the*** n = ***2 levels are exaggerated). The lowm-frequency*** A, ***and*** E ***transitions are obvious in the high-intensity spectrum, whereas the*** T_2 ***transition apparently overlaps the normal $0 \rightarrow \nu_3$ absorption.***

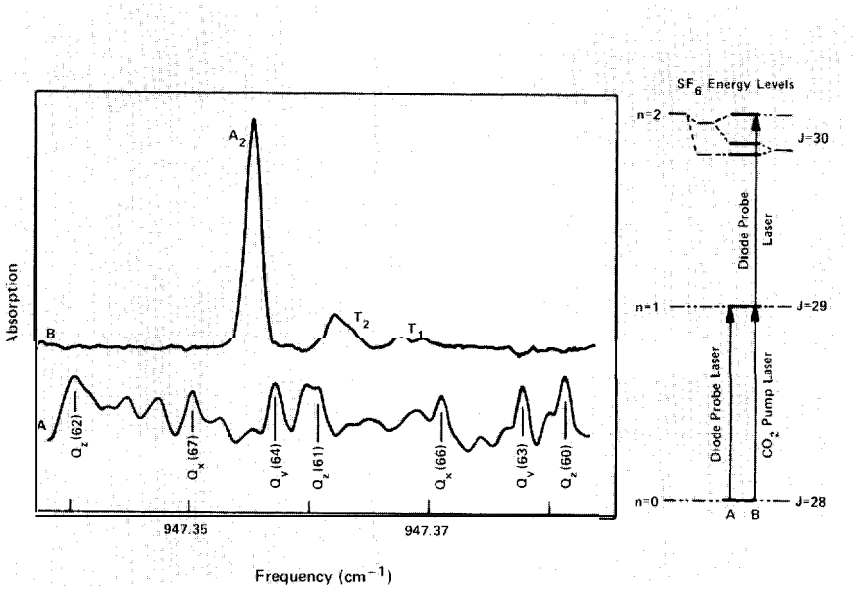

Fig 13. Trace B is a portion of the $\nu_3 \rightarrow 2\nu_3$ double-resonance spectrum of SF_6, recorded by P. F. Moulton and A. Mooradian at the MIT Lincoln Laboratory. A CO_2 laser pumps R (28) of ν_3, populating the J = 29 upper state, while the diode probe laser scans over the $\nu_3 \rightarrow 2\nu_3$ R(29) transition. The diode laser is able to resolve rotational fine structure, and this particular spectrum shows three of the four peaks of an $A_1T_1T_2A_2$ cluster. Trace A is a scan with the pump laser turned off; the resulting ν_3 Q-branch spectrum, similar to that of Fig. 2c, is used to calibrate the frequency.

have been determined, one can characterize the frequency dependence of the multiple-photon absorption. Figure 12 shows a comparison of the theoretical two-photon ($0 \rightarrow$ "ν_3" $\rightarrow 2\nu_3$) absorption spectrum of SF_6 with the high-intensity absorption actually observed using a tunable high-pressure CO_2 laser, In a two-photon resonance, in contrast to a single-photon ($0 \rightarrow 2\nu_3$) transition which is forbidden), both steps ($0 \rightarrow$ "ν_3" and "ν_3" $\rightarrow 2\nu_3$) are allowed, but the intermediate "ν_3" level is a virtual state that is detuned from the true position of ν_3; this two-photon resonance is shown in the upper set of energy levels of Fig. 12. The one-photon to ν_3 (black) and two-photon to $2\nu_3$ (shaded) spectra account for most of the features seen. The remaining features can be accounted for by higher-order multiphoton resonances. The three peaks in the calculated two-photon spectrum correspond to transitions to the A_1, E, and T_2 levels of $2\nu_3$. The fact that these absorption range from 944 cm^{-1} for A_1 up to 948 cm^{-1} for T_2 supports the idea discussed earlier that there are good pathways up the ladder at frequencies close to the fundamental at 948 cm-'. Similar analyses for UF_6 have led to predictions of the best pathways for dissociating this molecule in an isotonically selective manner.

With two lasers one can more easily probe the $2\nu_3$ levels of SF_6 by tuning the first laser to a real $0 + \nu_3$ transition and the second to allowed $\nu_3 \rightarrow 2\nu_3$ transitions. In such a double-resonance technique, the lasers are both tuned to a particular rotational J level for the intermediate ν_3 step: that is, one laser excites molecules into this J level at ν_3 while the second laser continues the excitation by pumping them out of that level and up to $2\nu_3$. The results of such an experiment are shown in Fig. 13. Here SF_6 is pumped by a CO_2 laser with peak intensity less than 1 kilowatt per square centimeter, so that only the v, rotational-vibrational levels are significantly populated and multiple-photon processes are minimized. The transient change in the absorption of a second (tunable diode) laser beam, caused by the presence of the pump signal, is recorded as the double-resonance signal. The three peaks in the figure represent a small portion of the rotational tine structure of the $\nu_3 \rightarrow 2\nu_3$ R (29) transition. The same constants used in the $3\nu_3$ analysis can be used to analyze the $2\nu_3$ spectrum as well. As a result, some 24 double-resonance signals have been assigned and the predicted $2\nu_3$ vibrational levels in Fig. 9 are now confirmed.

Although even higher anharmonicity contants become important further up the ladder ($n > 5$), we have used the constants X_{33}, G_{33}, and T_{33} to calculate the energy levels of $20\nu_3$ in order to elucidate the generic properties of the vibrational level splitting. In Fig. 14 are plotted the energy levels as a function of T_{33} ($G_{33} = 1.0$) such that the local-mode quantum numbers (n_x, n_y, n_z) describe the motion on the far left and the vibrational angular momentum quantum numbers ℓ describe the motion on the far right. One may think of this plot as representing UF_6 on the left, SiF_4 on the right, and SF_6 in the middle.

The levels are plotted in Fig. 14 with each class of symmetry species, A, E, and T, represented by a different color (red, green, and dark blue, respectively). Thus, whenever two or more symmetry species coincide or cluster, a new color is termed. For example, an *ATE* cluster mixes red, green, and dark blue to form a light yellow line while an $A_1T_1T_2A_2$ cluster results in a pink line.

Despite the fact that this analysis represents vibrational rather than rotational excitation, the various levels here appear to cluster as well. This is especially true on the near right for the t-dominated SiF_4 molecule, where the preponderance of pink $(A_1T_1T_2A_2)$ and light blue (T_1,ET_2) indicates vibrations quantized about the threefold symmetry axis while the dark blue (T_1T_2) indicate vibrations quantized about the fourfold axis. Also, surprisingly, the fourfold axis clusters seem to be conserved even in the intermediate region for SF_6.

The consequences of this for vibrational intramolecular relaxation and multiple-photon pathways are being investigated. In particular, transitions are strongly allowed only between energy levels of the same symmetry species. At the extreme right, with no splitting of energy levels, there is strong coupling between the many states of a given *f* level, and the density of states available for each vibrational energy transition is large. But as one moves to the left, the splitting breaks up the states into clusters of different symmetry. This clustering, in effect, reduces the density of states connected by vibrational transitions or other intramolecular processes because interactions should occur only between clusters of the same color.

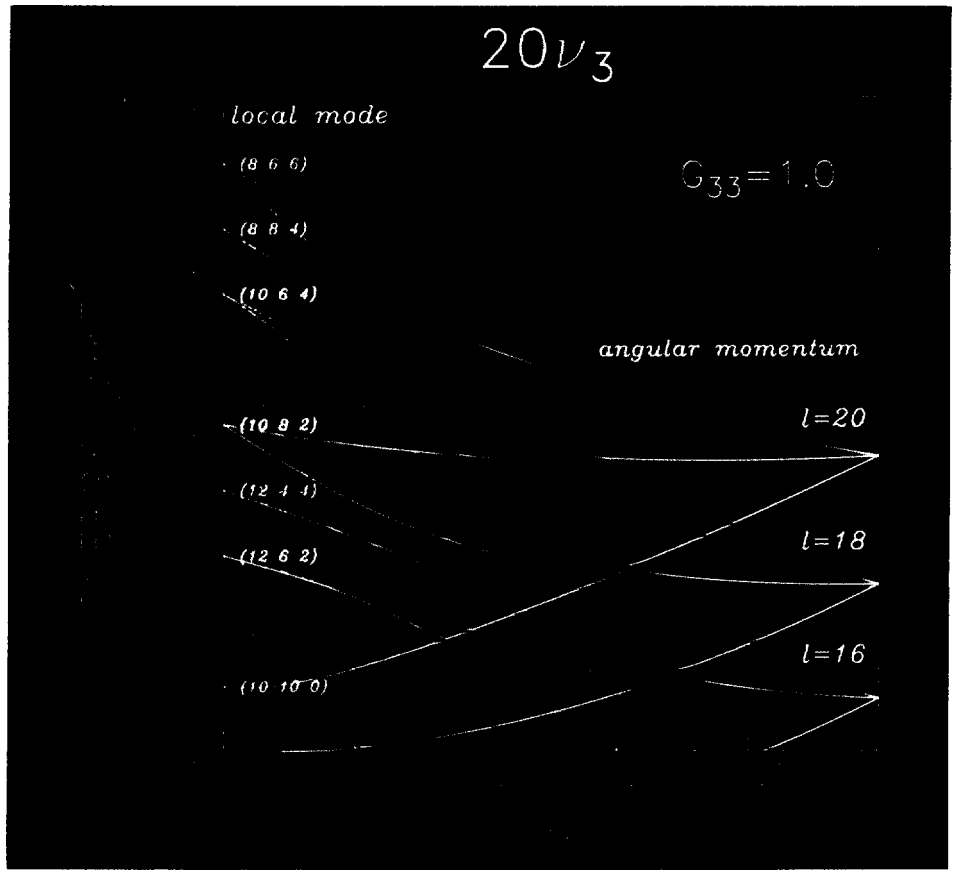

Fig. 14. Model enharmonic splitting in the overtone band $20\nu_3$. The vibrational energy levels shown here as a function of the anharmonicity constant T_{33} are represented with a different color for each class of symmetry species (A—red, E—green, and T—dark blue). Thus, the vibrational clustering of two or more symmetry species forms new colors with 4-fold clusters appearing as light yellow* (ATE) *and dark blue* (TT)*, and with 3-fold clusters appearing as light blue* (TET) *and pink* (ATTA)*. An angular-momentum dominated molecule such as SIF_4 would fall to the right of the graph while a local-mode molecule such as UF_6 would be to the left.

Reaping the Benefits

Once the energy-level code had been unraveled for the prototypical molecules, the spectra of other similar molecules became much easier to decode. One dramatic example was CF_4, a material that can be made to lase effectively in the photochemically important 630-cm-' (16-micrometer) region.

J. J. Tiee and C. Wittig first demonstrated in 1976 that when the $\nu_2 + \nu_4$ combination band of CF_4 near 1066 cm-' is pumped with a CO_2 laser, stimulated emission occurs on the $(\nu_2 + \nu_4) \rightarrow \nu_2$ transition (Fig. 15). However, since CF_4 is a heavy, tetrahedrally symmetric molecule, its vibrational bands consist of the typical array of finely spaced absorption. The actual CF_4 lasing frequency may range from 605 to 655 cm-], depending on the particular absorption pumped, While this large range of lasing frequencies is potentially an advantage, control and prediction of the actual lasing frequency is a problem. With a given pump frequency overlapping several absorption, lasing may occur at several widely separated frequencies, and the laser has a marked tendency to switch frequencies from moment to moment.

Analysis of the pump band absorption, $\nu_2 + \nu_4$, showed this degenerate vibrational state to be split by Coriolis forces. Recognition of the origin of the $\nu_2 + \nu_4$ structure led to detailed assignments for the absorption; selection rules for the lasing transitions

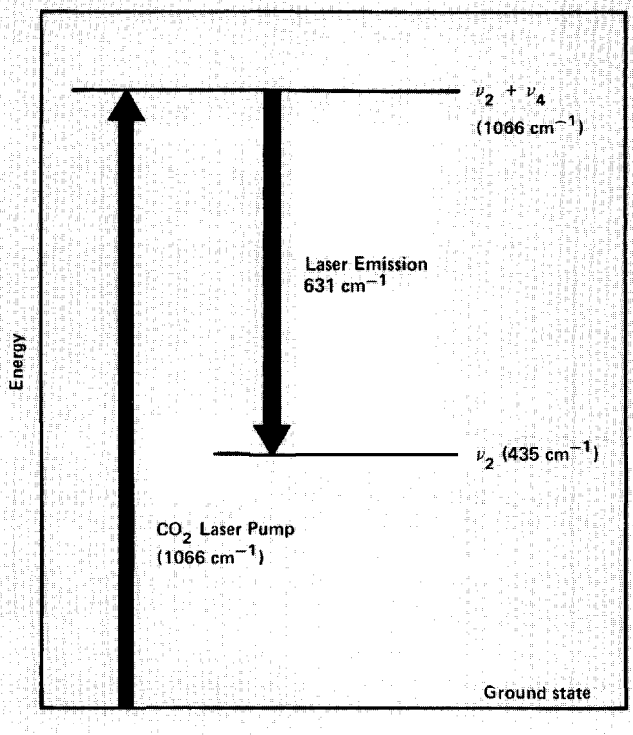

Fig. 15. Vibrational energy level diagram for the $C0_2$-pumped CF_4 laser.

TABLE I
BOND LENGTH IN CF_4

Vibrational State	C-F Bond Length (angstroms)
ground state	1.31943
ν_4	1.31907
ν_2	1.32062
$\nu_2 + \nu_4$	1.32028

that result from each absorption followed immediately. Using the molecular constants obtained from the $\nu_2 + \nu_4$ analysis and the frequencies of a few dozen known laser transitions, the assignments were made for the difference band $\nu_2 \rightarrow \nu_2 + \nu_4$. The final result was a frequency expression for the lasing transitions that predicts the strongest of these to within a few thousandths of a cm–', which is more accurate than can be measured at present.

The analysis discussed above has enabled the CF_4 laser to be designed to emit at specific frequencies that might be desirable in particular photochemical experiments. It has also enabled the frequencies of isotopic forms of CF_4 to be predicted. As a by-product of this analysis, the ground- and excited-state rotational constants have been separately determined, which is not possible from the infrared spectrum of a vibrational fundamental alone. From these the effective bond lengths in the various vibrational states can be obtained (Table I), all with an estimated uncertainty of ±0.00009 angstrom. These results should be compared with those obtained by diffraction methods, which are accurate to only a few thousandths of an angstrom at best, and give a bond length that is the effective average over all of the populated vibrational states.

The benefits of high-resolution laser spectroscopy are many. With CF_4, both precise molecular constants and the fine details of a lasing system are provided. With UF_6, the spectroscopy helps map the alternative pathways to photochemical dissociation necessary for the molecular isotope separation of uranium. The analyses of SF_6 and SiF_4 have led to a detailed understanding of the molecular energy levels that are pumped by $C0_2$ laser radiation in various nonlinear optical experiments. But perhaps the greatest benefits will come from our understanding of molecular dynamics, such as the insight that for heavy, symmetric molecules both rotational and vibrational motion are quantized about symmetry axes. ■

Acknowledgments

The Applied Photochemistry Division high-resolution spectroscopy program has drawn on the expertise of numerous people. It is a pleasure to thank our Los Alamos colleagues who have contributed to this work at one time or another: J. P. Aldridge, R. F. Begley, E. G. Brock, M. I. Buchwald, C. D. Cantrell, H. Filip, H. Flicker, H. W. Galbraith, R. F. Holland, C. R. Jones, R. C. Kennedy, K. C. Kim, B. J. Krohn, G. A. Laguna, J. D. Louck, N. G. Nereson, L. J. Radziemski, M. J. Reisfeld, D. M. Seitz, M. S. Sorem, J. M. Telle, and M. C. Vasquez. We also wish to acknowledge fruitful collaborations with P. Esherick and A. Owyoung (Sandia National Laboratories), K. Fox (University of Tennessee), L. Henry (University of Paris), E. D. Hinkley, A. Mooradian, and P. F. Moulton (the Massachusetts Institute of Technology Lincoln Laboratory), D. W. Magnuson and D. F. Smith (Oak Ridge Gaseous Diffusion Plant), J. Moret-Bailly (University of Dijon), J. Overend (University of Minnesota), W. B. Person (University of Florida), F. R. Petersen and J. S. Wells (National Bureau of Standards, Boulder), A. S. Pine (National Bureau of Standards, Gaithersburg), and A. G. Robiette (University of Reading).

Further Reading

J. I. Steinfeld, *Molecules and Radiation: An Introduction to Modern Molecular Spectroscopy* (Harper& Row, New York, 1974).

V. S. Letokhov, "Problems in Laser Spectroscopy," Soviet Physics Uspekhi (English Translation) 19, 109-136 (1 976).

M. J. Cones and C. R. Pidgeon, "Tunable Lasers," Reports on Progress in Physics 38,329-460 (1975).

C. R. Pidgeon and M. J. Cones, "Recent Developments in Tunable Lasers for Spectroscopy," Nature 279,377-381 (1979).

R. S. McDowell, "High Resolution Infrared Spectroscopy with Tunable Lasers," Advances in Infrared and Raman Spectroscopy 5, 1-66 (1978).

R. S. McDowell, "Vibrational Spectroscopy Using Tunable Lasers," Vibrational Spectra and Structure 10, 1-152 (1981).

J. D. Louck and H. W. Galbraith, "Eckart Vectors, Eckart Frames, and Polyatomic Molecules," Reviews of Modern Physics 48, 69-106 (1976).

W. G. Harter, C. W. Patterson, and F. J. da Paixao, "Frame Transformation Relations and Multipole Transitions in Symmetric Polyatomic Molecules," Reviews of Modern Physics 50,37-83 (1978).

W. G. Harter and C. W. Patterson, "Theory of Hyperfine and Superfine Levels in Symmetric Polyatomic Molecules. I. Trigonal and Tetrahedral Molecules: Elementary Spin- 1/2 Cases in Vibronic Ground States," Physical Review A 19,2277-2303 (1979).

W. G. Harter, "Theory of Hyperfine and Superfine Levels in Symmetric Polyatomic Molecules. II. Elementary Cases in Octahedral Hexafluoride Molecules," Physical Review A 24, 192-264 (1981).

H. W. Galbraith, C. W. Patterson, B. J. Krohn, and W. G. Harter, "Line Frequency Expressions for Triply Degenerate Fundamentals of Spherical Top Molecules Appropriate for Large Angular Momentum," Journal of Molecular Spectroscopy 73,475-493 (1978).

H. W. Galbraith and J. R. Ackerhalt, "Vibrational Excitation in Polyatomic Molecules," in *Laser-Induced Chemical Processes*, J. I. Steinfeld, Ed. (Plenum Press, New York, 1981), pp. 1-44.

C. W. Patterson, B. J. Krohn, and A. S. Pine, "Interacting Band Analysis of the High-Resolution Spectrum of the $3\nu_3$, Manifold of SF_6," Journal of Molecular Spectroscopy 88, 133-166 (1981).

C. W. Patterson, R. S. McDowell, P. F. Moulton, and A. Mooradian, "High-Resolution Double-Resonance Spectroscopy of $2\nu_3 \leftarrow \nu_3$ Transitions in SF_6," Optics Letters 6, 93-95 (1981).

R. S. McDowell, C. W. Patterson, C. R. Jones, M. I. Buchwald, and J. M, Telle, "Spectroscopy of the CF_4 Laser," Proceedings of the Society of Photo-Optical Instrumentation Engineers 190,262-269 (1979).

C. W. Patterson, R. S. McDowell, and N. G. Nereson, "Emission Frequencies of the CF_4 Laser," IEEE Journal of Quantum Electronics QE-16, 1164-1169 (1980).

AUTHORS

Robin S. ("Rod") McDowell is a molecular spectroscopist who has seen infrared resolving power increase a millionfold over the past 20 years and who was among the first to apply this capability to the detailed analysis of vibrational spectra. He received his Bacheolor of Arts from Haverford College in 1956 and spent two summers at Los Alamos while in graduate school at Massachusetts Institute of Technology. His work with Llewellyn H. Jones in the Inorganic Chemistry Group drew him back to Los Alamos after he obtained his Ph.D. in 1960. After 15 years in the Chemistry-Nuclear Chemistry Division, the spectroscopic opportunities offered by the development of tunable infrared lasers attracted him to Project Jumper, and he is now Assistant Group Leader of the Applied Photochemistry Division's Laser Chemistry Group. In 1975 he and Hal Galbraith first untangled and assigned the complex rotational-vibrational spectrum of SF_6, and he has continued to work on high-resolution infrared and Raman spectroscopy, the analysis of molecular energy levels, and spectroscopic applications to laser development. He has published 80 scientific papers, including two review articles on laser spectroscopy, and shared the Los Alamos Optical Society Award for the Outstanding LASL Paper in Optics in 1979. (Photo by Henry F. Ortega)

Chris W. Patterson was born in Los Angeles, California, on August 1, 1946. He received his Bachelor of Science and Ph.D. degrees in physics from the University of Southern California at Los Angeles in 1968 and 1974, respectively. From 1974 to 1977 he was an Assistant Professor at the Institute of Physics of the University of Campinas, Sao Paulo, Brazil, where he worked on the application of the unitary group to the electronic orbital theory of atoms and molecules. Since 1977 he has been a Staff Member in the Theoretical Division of the Laboratory. His recent work is on the theory of the rotational-vibrational and hyperfine structure of molecules and the modeling of optically pumped molecular lasers in support of the laser isotope separation program. He is a member of Phi Beta Kappa and the Los Alamos Chapter of the Optical Society of America, and shared the Los Alamos Optical Society Award for the Outstanding LASL Paper in Optics in 1979. He was recently named the 1982 recipient of the Coblentz Society Award, which is given in recognition of exceptional work by a molecular spectroscopist before the age of 35. (Photo by Henry F. Ortega)

William G. Harter is a Professor of physics at the Georgia Institute of Technology and a consultant for the Laboratory's Theoretical Division. He received the first doctorate in physics granted by the University of California at Irvine in 1967. After serving a postdoctoral term at Irvine, he joined the physics faculty at the University of Southern California, and in 1974 he took a position at the University of Campinas in Brazil. He was a Visiting Fellow of the Joint Institute for Laboratory Astrophysics at the University of Colorado in Boulder before assuming his present position in 1978. His research interests include symmetry analysis for spectroscopy, applications of permutation and unitary groups, and at present the theory of spectral clusters. Dr. Harter first saw the cluster problem presented by Los Alamos researchers at a symposium in 1975. After constructing some simple rotational cluster model solutions he began a collaboration with Los Alamos from which these models have been further developed and extended. Dr. Harter is even trying to make rotational group theory commercially successful. He is currently marketing a rotational group slide rule and will soon produce an unusual pocket sundial that predicts, among other things, how long human skin can stand the Los Alamos sun on any given day. (Photo by Sarah Harrell, Georgia Institute of Technology)